Detection of Abnormalities in MRI Images using Texture Analysis

Thesis submitted in

partial fulfillment of the requirement for the award of degree of

Master of Engineering
in
Electronics Instrumentation and Control

Submitted by:

Monika Arora

(80751014)

Under Esteemed Guidance of:

Dr. Yaduvir Singh

Associate Professor, EIED

Supervisor

Thapar University, Patiala

JUNE 2009

ELECTRICAL AND INSTRUMENTATION ENGINEERING DEPARTMENT
THAPAR UNIVERSITY
PATIALA – 147004

DECLARATION

*I hereby declare that the report entitled "**Detection of Abnormalities in MRI Images using Texture Analysis**" is an authentic record of my own work carried out as requirements for the award of degree of **Master of Engineering** in **Electronic Instrumentation & Control** at **Thapar University**, Patiala, under the guidance of **Dr. Yaduvir Singh** (Associate Professor, EIED) January to June 2009.*

Monika Arora

Date: 15-7-09

Roll. No. 80751014

It is certified that the above statement made by the student is correct to the best of my knowledge and belief.

15/07/09

Dr. Yaduvir Singh
Associate Professor, EIED
Supervisor
Thapar University, Patiala

S. Ghosh 15/7/09

Dr. Smarajit Ghosh
Professor & Head, EIED
Thapar University, Patiala.

Dr. R. K. Sharma 21/7
Dean of Academic Affairs
Thapar University, Patiala.

ACKNOWLEDGMENT

The real spirit of achieving a goal is through the way of excellence and austere discipline. I would have never succeeded in completing my task without the cooperation, encouragement and help provided to me by various personalities.

With deep sense of gratitude I express my sincere thanks to my esteemed and worthy supervisor, Dr. Yadwir Singh, Associate Professor Department of Electrical & Instrumentation Engineering, Thapar University, Patiala, for their valuable guidance in carrying out this work under their effective supervision, encouragement, enlightenment and cooperation.

I shall be failing in my duties if I do not express my deep sense of gratitude towards Dr. Smaragit Ghosh, Professor & Head of the Department of Electrical & Instrumentation Engineering, Thapar University, Patiala who has been a constant source of inspiration for me throughout this work.

I am also thankful to all the staff members of the Department for their full cooperation and help.

I am also grateful to Delta Radiology Center, Patiala for providing me the real images for test my code and verification of results.

This acknowledgement would be incomplete if I do not mention the emotional support and blessings provided by my friends.

My greatest thanks are to all who wished me success especially my parents, my brother and sister. Above all I render my gratitude to the ALMIGHTY who bestowed self-confidence, ability and strength in me to complete this work.

Place: Thapar University, Patiala
Date: 15-7-09

Monika Arora

ii

ABSTRACT

Medical imaging technique is most commonly used to visualize the internal structure and function of the body. Magnetic Resonance Imaging provides much greater contrast between the different soft tissues of the body than computed tomography (CT) does, making it especially useful in neurological (brain), musculoskeletal, cardiovascular, and oncological (cancer) imaging. It is an image processing based method and this method may not provide complete diagnosis through the scanned images or their machines as performed by the medical agents. So, this method can even detect the smallest abnormality even in the earliest stage which the scan may or may not detect.

Textures features of MR images have been provided. The analyses of both the normal and abnormal images are done. The ranges of both the types of images are calculated and then the comparison is performed between them. So, to determine the whether the abnormality is there or not in the image, its texture features are compared and the feature lying outside the range finally detects the abnormality in the biomedical image.

In this thesis different MR scans of patients are taken having abnormality in their brain. Five cases are observed, on the bases of their comparison, the result is obtained at the end indicating the whether the presence of abnormality in the image.

ORGANIZATION OF THESIS

The first chapter includes the computer vision system where feature extraction is being a part of it and texture models are shown. The second includes the review of literature. The third chapter is based on biomedical medical imaging techniques where magnetic resonance imaging is shown, it's working, and scanning is briefly shown. The next chapter is the completely based on texture segmentation. In this chapter extraction of information is done using texture segmentation. The fifth chapter includes the methodology and formulation used while extraction information from the image. The detailed explanation is done using flowchart and algorithm. The sixth chapter finally provides the conclusion and the results which lastly detects the type of the image whether normal or abnormal image.

TABLE OF CONTENTS

LIST OF FIGURES

LIST OF TABLES

LIST OF ABBREVIATIONS

PCA	Principal Component Analysis
GMRF	Gaussian Markov Random Fields
GRF	Gibb's Random Fields
RGB	Red Green Blue
MRI	Magnetic Resonance Imaging
NMRI	Nuclear Magnetic Resonance Imaging
CT	Computed Tomography
RF	Radio Frequency
MRT	Magnetic Resonance Tomography
2DFT	Two-Dimensional Fourier Transform
3DFT	Three-Dimensional Fourier Transform
EPI	Echo-Planar Imaging
CSF	Cerebrospinal Fluid
CBF	Cerebral Blood Flow
CBV	Cerebral Blood Volume
GRE	Gradient Echo
TR	Repetition Time
SE	Spin Echo
DTI	Diffusion Tensor Imaging
DWI	Diffusion Weighted Imaging
MRA	Magnetic Resonance Angiography
MRV	Magnetic Resonance Venography
PET	Positron Emission Tomograph
EEG	Electroencephalograph
fMRI	Functional Magnetic Resonance Imaging
MEG	Magneto Encephalography
LBR	Local Binary Pattern
MRF	Markov Random Field
GLCM	Gray-Level Co-occurrence Matrix

CHAPTER 1
INTRODUCTION

In the past decade computer graphics experienced a wave of activity in the area of image-based rendering as researchers explored the idea of capturing samples of the real world as images and using them to synthesize novel views rather than recreating the entire physical world from scratch. This, in turn, fueled interest in image-based texture synthesis algorithms. Such an algorithm should be able to take a sample of texture and generate an unlimited amount of image data which, while not exactly like the original, will be perceived by humans to be the same texture.

In computer graphics, early work on texture was inspired by research in texture analysis and very much influenced by statistics that is the use of global histograms of image features and psychophysics that is the use of multi-scale, multi-orientation filter banks. While the results for stochastic textures were very good, this class of algorithms was unable to deal well with more structured textures. This shortcoming was addressed by proposing a very different and extremely simple way of synthesizing textures locally, one-pixel-at-a-time. In recent years this algorithm has been used for synthesizing a large spectrum of textures as well as filling holes in textured regions. It showed that similarly good results can be obtained by an even simpler (and much faster) procedure of quilting together patches of the input texture. Moreover, a method was demonstrated that transferred texture from one object onto another.

1.1 COMPUTER VISION SYSTEMS

The organization of a computer vision system is highly application dependent. Some systems are stand-alone applications which solve a specific measurement or detection problem, while other constitute a sub-system of a larger design which, for example, also contains sub-systems for control of mechanical actuators, planning, information databases, man-machine interfaces, etc. The specific implementation of a computer vision system also depends on if its functionality is pre-specified or if some part of it can

be learned or modified during operation. There are, however, typical functions which are found in many computer vision systems. These are:

1. Image Acquisition
2. Pre-processing
3. Feature Extraction
4. Detection/Segmentation
5. High Level Processing

1.1.1 IMAGE ACQUISITION

A digital image is produced by one or several image sensors, which, besides various types of light-sensitive cameras, include range sensors, tomography devices, radar, ultra-sonic cameras, etc. Depending on the type of sensor, the resulting image data is an ordinary 2D image, a 3D volume, or an image sequence. The pixel values typically correspond to light intensity in one or several spectral bands (gray images or colour images), but can also be related to various physical measures, such as depth, absorption or reflectance of sonic or electromagnetic waves, or nuclear magnetic resonance.

1.1.2 PRE-PROCESSING

Before a computer vision method can be applied to image data in order to extract some specific piece of information, it is usually necessary to process the data in order to assure that it satisfies certain assumptions implied by the method.

Texture analysis was very much influenced by statistics that is the use of global histograms of image features and psychophysics that is the use of multi-scale, multi-orientation filter banks.

Examples are:

1. Re-sampling in order to assure that the image coordinate system is correct.
2. Noise reduction in order to assure that sensor noise does not introduce false information.
3. Contrast enhancement to assure that relevant information can be detected.
4. Scale-space representation to enhance image structures at locally appropriate scales.

1.1.3 FEATURE EXTRACTION

Image features at various levels of complexity are extracted from the image data.

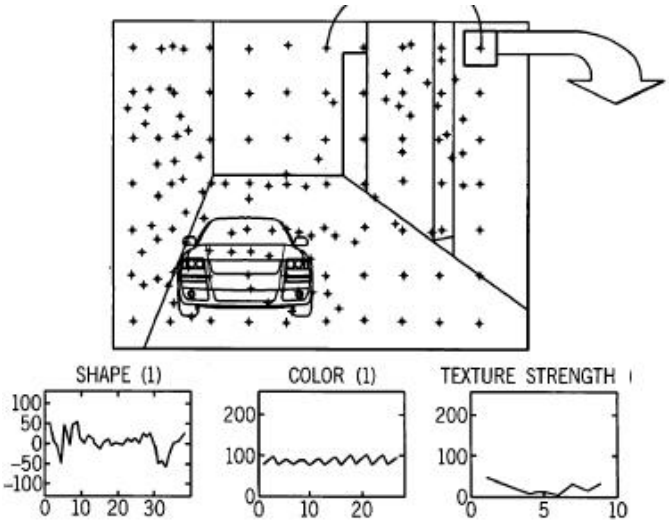

Figure1.1: Image Feature Extraction

Typical examples of such features are

1. Lines, edges and ridges.
2. Localized interest points such as corners, blobs or points. More complex features may be related to texture, shape or motion.

1.1.4 DETECTION/SEGMENTATION

At some point in the processing a decision is made about which image points or regions of the image are relevant for further processing. Examples are

1. Selection of a specific set of interest points.
2. Segmentation of one or multiple image regions which contain a specific object of interest.

1.1.5 HIGH-LEVEL PROCESSING

At this step the input is typically a small set of data, for example a set of points or an image region which is assumed to contain a specific object. The remaining processing deals with, for example:

1. Verification that the data satisfy model-based and application specific assumptions.
2. Estimation of application specific parameters, such as object pose or object size.
3. Classifying a detected object into different categories.

1.2 FEATURE EXTRACTION

In pattern recognition and in image processing, feature extraction is a special form of dimensionality reduction. When the input data to an algorithm is too large to be processed and it is suspected to be notoriously redundant (much data, but not much information) then the input data will be transformed into a reduced representation set of features (also named features vector). Transforming the input data into the set of features is called features extraction. If the features extracted are carefully chosen it is expected that the features set will extract the relevant information from the input data in order to perform the desired task using this reduced representation instead of the full size input.

1.2.1 GENERAL

Feature extraction involves simplifying the amount of resources required to describe a large set of data accurately. When performing analysis of complex data one of the major problems stems from the number of variables involved. Analysis with a large number of variables generally requires a large amount of memory and computation power or a classification algorithm which overfits the training sample and generalizes poorly to new samples. Feature extraction is a general term for methods of constructing combinations of the variables to get around these problems while still describing the data with sufficient accuracy.

Best results are achieved when an expert constructs a set of application-dependent features. Nevertheless, if no such expert knowledge is available general dimensionality reduction techniques may help. These include:

1. Principal components analysis.
2. Semidefinite embedding
3. Multifactor dimensionality reduction
4. Nonlinear dimensionality reduction
5. Isomap
6. Kernel PCA
7. Latent semantic analysis
8. Partial least squares
9. Independent Component Analysis.

1.3 IMAGE PROCESSING

It can be used in the area of image processing which involves using algorithms to detect and isolate various desired portions or shapes (features) of a digitized image or video stream. It is particularly important in the area of Optical Character Recognition

Low-Level:-

1. Edge detection
2. Corner detection
3. Blob detection
4. Ridge detection
5. Scale-invariant feature transform.
6. Texture segmentation

1.3.1 EDGES

Edges are points where there is a boundary (or an edge) between two image regions. In general, an edge can be of almost arbitrary shape, and may include junctions. In practice, edges are usually defined as sets of points in the image which have a strong gradient magnitude.

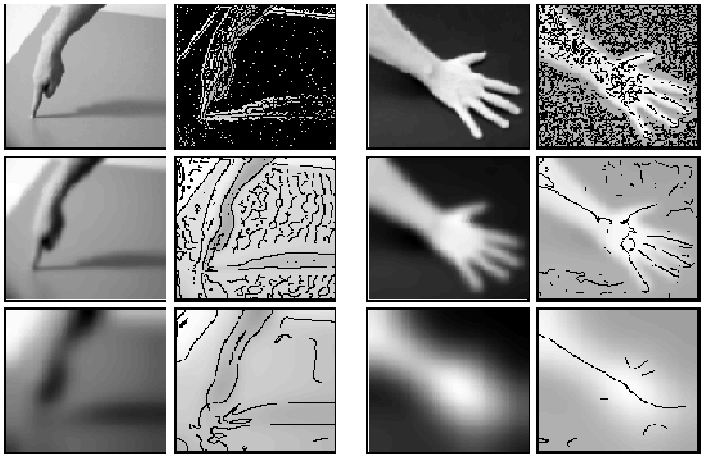

Figure 1.2: Edge Detection

Furthermore, some common algorithms will then chain high gradient points together to form a more complete description of an edge. These algorithms usually place some constraints on the properties of an edge, such as shape, smoothness, and gradient value. Locally, edges have a one dimensional structure.

1.3.2 CORNERS / INTEREST POINTS

The terms corners and interest points are used somewhat interchangeably and refer to point-like features in an image, which have a local two dimensional structure. The name "Corner" arose since early algorithms first performed edge detection, and then analyzed the edges to find rapid changes in direction (corners). These algorithms were then developed so that explicit edge detection was no longer required, for instance by looking for high levels of curvature in the image gradient. It was then noticed that the so-called corners were also being detected on parts of the image which were not corners in the traditional sense (for instance a small bright spot on a dark background may be detected). These points are frequently known as interest points, but the term "corner" is used by tradition.

1.3.3 BLOBS / REGIONS OF INTEREST OR INTEREST POINTS

Blobs provide a complementary description of image structures in terms of regions, as opposed to corners that are more point-like. Nevertheless, blob descriptors often contain a preferred point (a local maximum of an operator response or a center of gravity) which means that many blob detectors may also be regarded as interest point operators. Blob detectors can detect areas in an image which are too smooth to be detected by a corner detector.

Consider shrinking an image and then performing corner detection. The detector will respond to points which are sharp in the shrunk image, but may be smooth in the original image. It is at this point that the difference between a corner detector and a blob detector becomes somewhat vague. To a large extent, this distinction can be remedied by including an appropriate notion of scale. Nevertheless, due to their response properties to different types of image structures at different scales, the LoG and DoH blob detectors are also mentioned in the article on corner detection.

1.3.4 RIDGES

For elongated objects, the notion of ridges is a natural tool. A ridge descriptor computed from a grey-level image can be seen as a generalization of a medial axis. From a practical viewpoint, a ridge can be thought of as a one-dimensional curve that represents an axis of symmetry, and in addition has an attribute of local ridge width associated with each ridge

point. Unfortunately, however, it is algorithmically harder to extract ridge features from general classes of grey-level images than edge-, corner- or blob features. Nevertheless, ridge descriptors are frequently used for road extraction in aerial images and for extracting blood vessels in medical images.

1.3.5 TEXTURE SEGEMENTATION

The partitioning of an image into regions, each of which contains a single texture distinct from its neighbors. Segmentation has at least a formal definition, texture has less of one. A typical definition is one or more basic local patterns that are repeated in a periodic manner. However, it is not clear exactly what the pattern is or how it is repeated. It is not even clear whether texture is an inherent property of all things, or whether some objects or regions lack texture altogether.

There are two approaches to defining texture, which may be thought of as ``top-down'' and ``bottom-up.'' Top-down models claim that there is a basic element, called a texel or a texton, and a placement rule, and the rule defines how and where the elements are placed. This definition works well if the texture consists of bricks. The bottom-up approach claims that texture is a property that can be derived from the statistics of small groups of pixels, such as mean and variance. This works better for textures like quartz and grass where it is difficult to see individual elements. The dividing line between the two approaches is by no means clear. Two different objects with a common boundary may have the same texture and be lumped together, which may or may not be desired. Texture segmentation will invariably break up certain objects which contain multiple textures, and group together pieces of different objects into one region.

1.4 TEXTURE MODELS

There is no shortage of texture models to choose from. Since no particular representation has been shown to give great results on a wide range of textures, many ideas have been tried. Some have been created from scratch, while others have been borrowed from other disciplines. Models are often conceived by thinking of the image not as a set of pixels, but rather as a function I(x,y) defined over a continuous region of the plane.

In general, the purpose of a texture model is to provide a means for transforming a window of an image into a set of numbers, which in this paper will be called a feature vector. The feature vector can be thought of as a point in an *n*-dimensional feature space. The representation is good, then, if windows taken from the same texture sample form a cluster in feature space, and if windows taken from different texture samples are far away from each other in feature space. An inherent problem to be noted is that as we move across a boundary from one texture to another, the vectors do not travel in a straight line from one cluster to the other; in fact, they may cross a region of feature space belonging to an entirely different texture.

The models can be roughly divided into three main categories:

1. Image pyramids: which try to capture spatial frequencies at different scales.
2. Random fields: which assume that pixel values are chosen by a two-dimensional stochastic process and
3. Statistical methods: a catch-all phrase to group together a number of older techniques which are not as popular as the first two groups.

1.4.1 IMAGE PYRAMIDS

The idea behind image pyramids is to generate a number of homogeneous parameters that represent the response of a bank of filters at different scales and possibly different orientations. There are many different types of filters that can be used for this purpose. One of the simplest types of filters is the Laplacian. It is a symmetrical filter, consisting of a highly positive center region and a negative ``surround." It is over-complete, however, meaning that some of the information encoded is redundant, and therefore the original signal cannot recover from the representation.

Gabor filters are topologically similar to Laplacian filters, but they are elliptical rather than round, and they are highly eccentric. As such, they can be set at different orientations within the same scale, allowing possible detection of rotated versions of the same texture. Wavelets are another type of filter family. They are constructed from a mother wavelet, which can be any admissible function (a function with no DC component; the Fourier transform of that function evaluated at 0 is 0). A family is constructed by dilating and translating the mother wavelet by different amounts. The

advantage over simply using the Fourier transform for frequency analysis is that wavelets respond better to discontinuities (that is, edges) and spikes.

The most flexible of the image pyramids, however, are the steerable pyramids. Steerable pyramids can be thought of as an over-complete wavelet transform. They are called steerable because, by using only a small number of filters corresponding to a few directions, the output of a filter in any direction can easily be computed as a weighted sum of the filters that have already been calculated. In addition, steerable pyramids mostly avoid the problem of aliasing, or the confusion of low and high frequency components.

1.4.2 RANDOM FIELDS

The idea behind random fields is that the value at each pixel is chosen by a two-dimensional stochastic process. Imagine removing one pixel from an image. Given a type of probability distribution and all the other pixels in the image, we can determine the most likely parameters of that distribution. From the parameters we can express the probability that the missing pixel has any one particular value.

Obviously, performing this calculation would be very expensive and of little use, since the random field model for texture segmentation assumes that different regions of the image have their pixel values drawn from different distributions. Fortunately, we have the Markov property, which is stated as follows: the probability that a pixel has a certain grey level given every other pixel in the image is equal to the probability that the pixel has that same grey level given only the pixels in a neighborhood surrounding that pixel. The probability distribution is often chosen to be Gaussian, resulting in a special class of random fields called Gaussian Markov Random Fields, or GMRF's. Some parameters that can be computed from GMRFs are mean, variance, and autocovariance in different directions. Another important relative is known as Gibbs Random Fields, or GRF's. GRFs also obey the Markov property, but they use an exponential probability distribution that is derived from an energy function. The energy function is estimated by looking at small neighborhoods called cliques (sometimes as small as pairs of pixels). Each clique contributes one parameter to the distribution.

1.4.3 STATISTICAL MODELS

The aforementioned models are currently the most popular for describing textures. In addition, there are a number of other models for analyzing textures, and while they might not be as popular as the above models, they are by no means useless. Co-occurrence matrices, also called Spatial Grey Level Dependence Matrices, attempt to capture texture using a sparse representation. Each matrix in the set corresponds to an offset (e.g. 2 pixels down and 1 pixel to the left).

The entry in row i and column j of each matrix is the number of pixels in the image of grey level i that have a neighbor of grey level j in the direction of the offset. From these matrices a number of statistical quantities can be measured, such as mean, variance, entropy, energy, contrast, and correlation. The auto-correlation measure in statistics determines how a function varies with itself as it is displaced from the origin. When applied to images, auto-correlation can be used as a measure of the coarseness of textures in different directions.

The Discrete Fourier Transform and the Discrete Cosine Transform are two examples of a general class of mathematical techniques called orthogonal transforms. This set includes some of the filters mentioned in conjunction with image pyramids, such as the Haar transform. In general, a set of orthogonal basis functions is generated, and then each function is convolved with the image to yield a set of numbers at each point. Textures have also been discriminated on the basis of how many edges fall within a unit area, or how many relative extrema falls within a unit area. A relative extremum in an image is simply a pixel whose grey-level value is higher (or lower) than those of all its immediate neighbors.

Fractals are very important and they are used for analyzing which can be implemented to many other applications. They are sometimes used for texture analysis and segmentation because, like texture, fractals have inherent scales attached to them. Rather than guessing at a scale at which the analysis should proceed, a fractal analysis can yield the fractal dimension of a texture, which should indicate the scale.

1.5 TEXTURE ANALYSIS AND SYNTHESIS

Texture is a ubiquitous visual experience. It can describe a wide variety of surface characteristics such as terrain, plants, minerals, fur and skin. Since reproducing the visual realism of the real world is a major goal for computer graphics, textures are commonly employed when rendering synthetic images. These textures can be obtained from a variety of sources such as hand-drawn pictures or scanned photographs. Hand-drawn pictures can be aesthetically pleasing, but it is hard to make them photo-realistic. Most scanned images, however, are of inadequate size and can lead to visible seams or repetition if they are directly used for texture mapping. Texture synthesis is an alternative way to create textures. Because synthetic textures can be made of any size, visual repetition is avoided. Texture synthesis can also produce tileable images by properly handling the boundary conditions. Potential applications of texture synthesis are also broad; some examples are image de-noising, occlusion fill-in, and compression.

The problem of texture synthesis can be stated as follows: Given a texture sample, synthesize a new texture that, when perceived by a human observer, appears to be generated by the same underlying stochastic process. An example is shown in the above figure. Our goal is to develop a new texture synthesis algorithm that is efficient, general, user-friendly, and able to produce high quality textures. In addition, we would like to extend the horizon of texture synthesis by exploring a variety of new applications based on our algorithm.

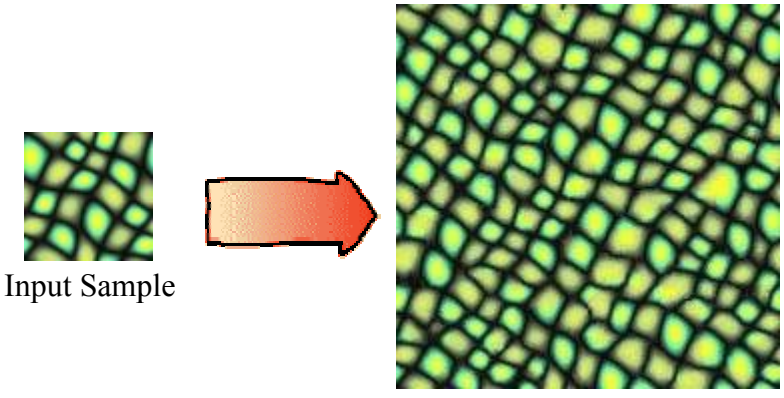

Figure 1.3: Conversion of image into synthesized image

1.6 IMAGE RETRIEVAL

There are numerous image retrieval algorithms which use texture/shape extraction to retrieve images from database. These techniques work basically on grayscale images. Thus to retrieve color images researchers have used a color extraction process in addition to one of the texture/shape extraction process. Texture extraction process could be used to retrieve color images.

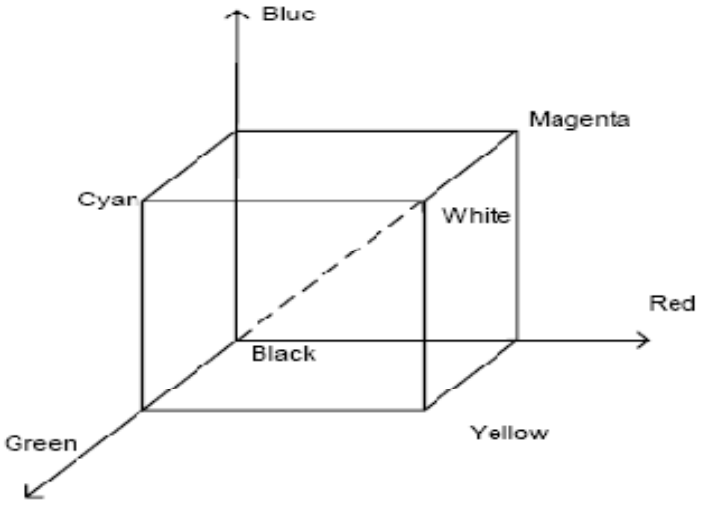

Figure 1.4: RGB color

The main purpose of image retrieval is to retrieve a set of images matching the query and the best match always should be ranked highest otherwise it defeats the whole purpose of image retrieval. As seen from Fig. 1.5, color image consists of three layers i.e. Red, Green and Blue (RGB). The color composition could be represented in a RGB space, Figure 1.4. The diagonal running through the space is the grayscale area. From the RGB space we can see that any color is a combination of red, green and blue elements. A basic color image could be described as three layered image with each layer as red, green and blue. When a particular area of a color image is considered, then there could be different color combinations with respect to other areas of the image. An area with yellow would have a combination of red and green color elements only. Similarly an area with magenta would have combination of red and blue elements only. Thus if an image of an object is considered yellow color, then the object is best described in red and green layers, not in blue layer. Hence, certain features are unique and distinct to each color layer for a particular image, depending on the color composition.

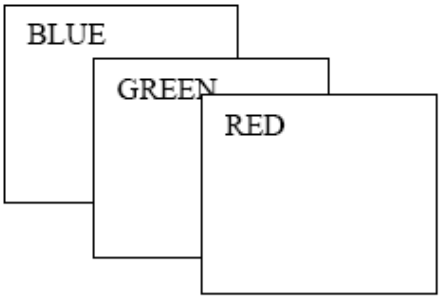

Figure 1.5: Three layers of a color image

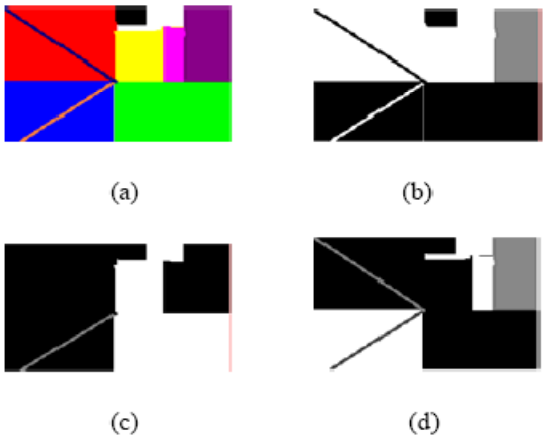

Figure 1.6: (a) Different layers of the color image: (b) Red layer, (c) Green layer, (d) Blue layer images

Main objective of a texture/shape extraction process is to extract the prominent feature of an image. Thus if a query image has prominent features only in red layer and green layer, we could conclude that the image is some sort of combination of red and green elements, not blue. To get a better understanding of the process let us consider a color image. Certain texture/shape features which appear in the red layer does not appear with the same intensity in the green or blue layers and vice versa is also true. Therefore by extracting feature vectors from each layer separately and matching the same with the database feature vectors, then the best match features in red layer, green layer and blue layer respectively is obtained. Hence, if the feature vectors of each layer of the query have matched with feature vectors of each layer of a particular image in the database; then it is concluded that the query image has a similar RGB structure compared the image from database or in other words suggesting that the query image color composition has matched with a color composition of an image in database. This would provide us with better ranking and effective retrieval of color images.

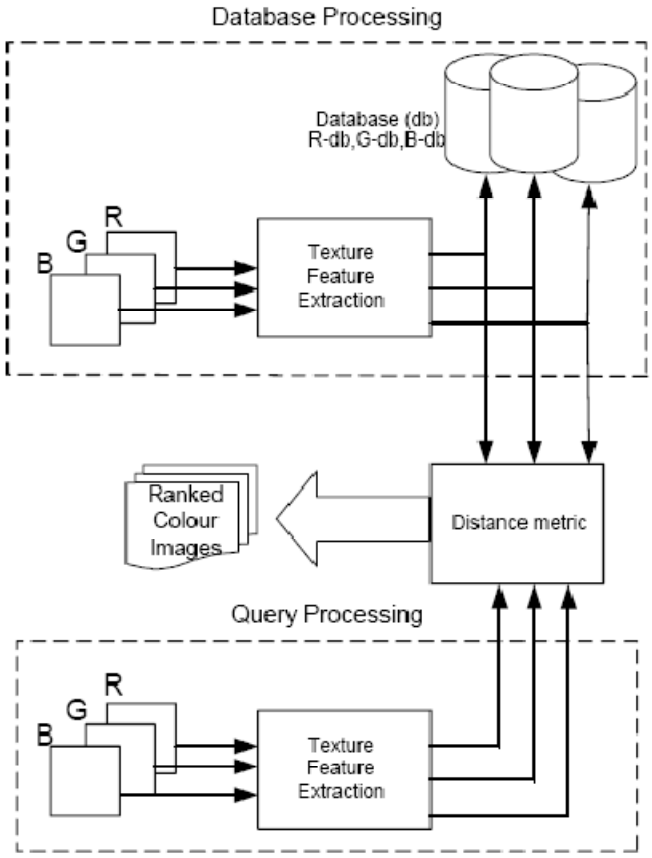

Figure1.7: Overview of the entire system

We feed each layer of the RGB image separately to texture extraction process and store the feature vectors corresponding to each layer in the feature vector database. We perform the same process on the query image and then calculate the distance metric for each respective feature vectors from respective layers. Based on each layer we get three different rankings, a simple average is calculated to derive the final ranking for the retrieved images. Certain texture/shape features which appear in the red layer does not appear with the same intensity in the green or blue layers and vice versa is also true

However the problem arises from the fact that while using texture extraction process the system would not have any idea about the color composition of the image. Using a texture extraction process alone to retrieve color images, would result in badly ranked recalls (e.g. best match for the query in terms of color composition may be placed as the lowest ranked image).

1.7 CONCLUSION

Texture Extraction is a part of feature extraction which is a special form of dimensionality reduction. For a large input data to an algorithm to be processed and it is suspected to be notoriously redundant then the transformation of input data into a reduced representation set of features will be produced. Transforming the input data into the set of features is called features extraction. If the features extracted are carefully chosen it is expected that the features set will extract the relevant information from the input data in order to perform the desired task using this reduced representation instead of the full size input.

CHAPTER 2
LITERATURE REVIEW

This chapter provides brief overview of work done in this area.

Wu Jianchao et.al (1989) described the technique for segmenting B-scan images, which is based on the concept of Module. Gray level sum and difference histogram were employed to extract texture features Module and Mode. Then K-mean clustering algorithm is used to partition B-scan image into homogenous zones of texture. The performance of this method is tested by the analysis of natural texture. Finally the author applied it to the abdominal ultrasound B-scan images. In this paper, a method that enabled partitioning of ultrasound B-scan images is proposed, each of which can then be characterized by Module and Mode two-dimensional distribution of the class to which it belongs. It allows contour extraction between textures, area measurement and tissue characterization in a non-rectangular window. The authors developed a new method to overcome the shortage of the features by making the texture features, derived from local gray-level histogram, contain the spatial information of pixels, on which the performance of segmentation based upon [1].

Kah-Chan Low (1990) presented an algorithm for labeling image regions based on pixel-level statistical pattern recognition. The structure of multiscale regions about each pixel is measured using isotropic Gaussian filters and by a Multiscale Orientation Field. In his work, the author created a redundant feature space representing several aspects of image structure across scale, orientation, and space and also emphasized on segmentation algorithm that decides the membership of pixels in regions using simple statistical pattern recognition methods such as distance measurement and thresholding. Feature vectors were examined locally to determine region membership; the features incorporate multiscale image structure information. Results of multiscale image segmentations on biomedical images were presented. The formal techniques employed the statistical pattern recognition paradigm. The processing used in the entire process was also characterized by their simplicity (or simple-mindedness). Because of this attribute, each of them, while quite effective in extracting image features for which they are designed,

do produce some segmentation errors in image areas that they were not equipped to handle. However, when their resulting and erroneous segmentations were combined in a simple manner, unexpectedly good primitive region segmentations were obtained [2].

N. A. Mohamed et.al (1999) described the application of fuzzy set theory in medical imaging, namely the segmentation of brain images. In his work, the author proposed a fully automatic technique to obtain image clusters. A modified fuzzy c-mean (FCM) classification algorithm is used to provide a fuzzy partition. A new method, inspired from the Markov random field (MRF), is less sensitive to noise as it filters the image while clustering it, and the filter parameters were enhanced in each iteration by the clustering process. A new method on a noisy CT scan and on a single channel MRI scan was applied and a methodology of over segmentation to the textured MRI scan was recommended. One of the applications of this technique is TBI recovery prediction in which it is important to consider the partial volume. The system stabilizes after a number of iterations with the membership value of the region contours reflecting the partial volume value. The final stage of the process is devoted to decision making or the defuzzification process [3].

John E. Koss et.al (1999) proposed to form images based on second-order statistical texture transforms (Haralick transforms) of a CT or MRI scan. The original scan plus the suite of texture transforms are then input into a Hopfield neural network (HNN). The network is constructed to solve an optimization problem, where the best solution is the minima of a Lyapunov energy function. On a sample abdominal CT scan, 79–100% of the pixels of seven abdominal organsand were clusttered which being the first to automate segmentation. Active contouring (e.g., SNAKE's) or a back-propagation neural network could then be used to assign names to the clusters and could be filled in the incorrectly clustered pixels. This first attempt at segmenting abdominal organs using texture transforms and ANN's correctly segmented over 90% of the pixels for most organs. This method could also be extended to three dimensions [4].

George York (1999) focused on the various algorithms, processing requirements, and the challenges of the ultrasound modes. Mature B and color-flow modes could be systolically implemented using hardwired components and boards, new applications, such as three-

dimensional imaging and image feature extraction, were being implemented more by using programmable processors. In this paper, the advantages of quick implementation of new applications without any additional hardware and the flexibility to adapt to the changing requirements of the dynamic new applications were offered [5].

Ewout Vansteenkiste et.al (2001) presented a technique for segmenting the affected tissue visible as white flaring in the ultrasound brain images of neonates with Leukomalacia (White Matter Damage). The technique combines both textural information of the investigated tissue as well as mathematical morphology in order to detect and delineate the boundaries of the affected parts of the brain. The reproducibility of the proposed technique was evaluated and the experimental results were validated by comparing them to the manual delineations of 12 expert medical doctors from different institutions. Although it appeared hard to reach a consensus on the correct segmentation of the flaring, because of the lack of a golden standard in the ultrasound images. In this paper, a much accurate method that outperformed the existing techniques which was based on active contours in speed was shown [6].

Stewart A. Levin (2002) focused on methods for analyzing images for important features and extracting qualitative and quantitative results. All three disciplines that participated in the workshop geophysics, medicine, and space-based remote sensing had an escalating need to automatically extract information from digital images and speakers in all three fields testified to the commonality of techniques and synergies among disciplines [7].

Alain Pitiot et.al (2002) presented a fully automated segmentation method for medical images. The goal is to localize and parameterize a variety of types of structure in these images for subsequent quantitative analysis. In this paper, a new hybrid strategy that combines a general elastic template matching approach and an evolutionary heuristic is proposed. The evolutionary algorithm uses prior statistical information about the shape of the target structure to control the behavior of a number of deformable templates. Each template, modeled in the form of a spline, is warped in a potential field which is itself dynamically adapted. Such a hybrid scheme proved to be promising: by maintaining a population of templates. Several optimization schemes and multivariate relations between the parameters of deformation model were developed. Adaptive approaches modified the

control parameters of deformable templates in response to contextual information and used time-dependent criteria that presented advantages in the progressive refinement and understanding of template matching methods [8].

Zumray Dokur (2002) presented a hybrid neural network for the segmentation of ultrasound images. Feature vectors were formed by the discrete cosine transform of pixel intensities in region of interest (ROI). The elements and the dimension of the feature vectors were determined by considering only two parameters: The amount of ignored coefficients and the dimension of the ROI. First-layer-nodes of the proposed hybrid network represented hyperspheres (HSs) in the feature space. Feature space was partitioned by intersecting these HSs to represent the distribution of classes. The locations and radii of the HSs were found by the genetic algorithms. Restricted Coulomb energy (RCE) network, modified RCE network; multi-layer perceptron and the proposed hybrid neural network were examined comparatively for the segmentation of ultrasound images [9].

Djamal Boukerroui et.al (2003) proposed a robust adaptive region segmentation algorithm for noisy images, within a Bayesian framework. A multiresolution implementation of the algorithm was performed using a wavelets basis and can be used to process both 2D and 3D data. In this paper, the adaptive character of the algorithm is focused and discussed how global and local statistics can be utilized in the segmentation process. An improvement on the adaptivity is proposed by introducing an enhancement to control the adaptive properties of the segmentation process. It took the form of a weighting function accounting for both local and global statistics, and is introduced in the minimization. A new formulation of the segmentation problem allowed to control the effective contribution of each statistical component. The segmentation algorithm is demonstrated on synthetic data, 2D breast ultrasound data and on echocardiographic sequences (2D + T). An evaluation of the performance of the proposed algorithm is also presented [10].

Russell Muzzolini (2003) proposed new multiresolution texture segmentation (MTS) approach which presented the issues of texture characterization, image resolution, and time to complete the segmentation. This approach generalized the conventional simulated

annealing method to a multiresolution framework and minimized an energy function which is dependent on the resolution of the size of the texture blocks in an image. Based on a priori information, the MTS algorithm selected the best feature to determine if a texture block is homogeneous or not. If it is homogeneous, then no splitting is required; otherwise splitting of the texture is performed. Based on a similar argument, merging is performed by examining the similarity of a texture block with its neighbors. A rigorous experimental procedure is also proposed to demonstrate the advantages of the proposed MTS approach on

1) The accuracy of the segmentation,

2) The efficiency of the algorithm, and

3) The use of varying features at different resolution.

Semireal images, created by sampling a series of diagnostic ultrasound images of an ovary in vitro, were tested to produce statistical measures on the performance of the approach. The ultrasound images themselves were then segmented to determine if the approach could achieve accurate results for the intended ultrasound application. The resulting segmentations of the ultrasound images can also be transformed into a three-dimensional model of a follicle thus providing a nondestructive means of examining the follicle in much more detail than is available in a two-dimensional cross section [11].

S. S. Mohamed et.al (2003) agreed that the conventional Trans-Rectal Ultrasound (TRUS) examination is an important, costeffective and useful technique for imaging the prostate. TRUS is used in the interpretation of the PSA assay, for monitoring response to nonsurgical and surgical therapy, and for providing image guidance during some minimally invasive procedures. In this paper, multi-channel filtering method is proposed which being an excellent method for prostate texture investigation. By processing the TRUS images using multiple resolution techniques, the image is decomposed into appropriate texture features that can be used to classify the textures accordingly. Using Human Visual system (HVS three features for texture analysis were used, mainly repetition, directionality and complexity. A bank of Gabor fi1ters that is well distributed to cover the entire frequency plane is designed to mimic the HVS and therefore it is an excellent tool that can be used for prostate texture segmentation. Some of the feature extraction methods were applied. Among these, the magnitude response that seemed to

produce the most accurate partitioning of the image. Another important post-filtering operation is smoothing of the filter outputs. A Gaussian smoother that matches the Gaussian of the filter is used to smooth the output image. Smoothing resulted in suppressing the variations within the same texture region in the output image, thus enhancing the segmentation process significantly [12].

Stuart S. C. Burnett et.al (2004) developed a deformable-template algorithm for the semi-automatic delineation of normal tissue structures on computed tomography images. In this paper, a method is illustrated by applying it to the spinal canal. Segmentation is performed in three steps:

1. Partial delineation of the anatomic structure is obtained by wavelet-based edge detection;
2. A deformable-model template is fitted to the edge set by chamfer matching; and
3. The template is relaxed away from its original shape into its final position. Appropriately chosen ranges for the model parameters limit the deformations of the template, accounting for interpatient variability. The spinal canal was modeled using Fourier descriptors derived from four sets of manually drawn contours. Segmentation was carried out, without manual intervention, on five CT data sets and the algorithm's performance was judged subjectively by two radiation oncologists. Two assessments were considered: in the first, segmentation on a random selection of 100 axial CT images was compared with the corresponding contours drawn manually by one of six dosimetrists, also chosen randomly; in the second assessment, the segmentation of each image in the five evaluable CT sets, a total of 557 axial images were rated as either successful, unsuccessful, or requiring further editing. Contours generated by the algorithm were more likely than manually drawn contours to be considered acceptable by the oncologists. The mean proportions of acceptable contours were 93% automatic and 69% manual. Automatic delineation of the spinal canal was deemed to be successful on 91% of the images, unsuccessful on 2% of the images, and requiring further editing on 7% of the images. Our deformable template algorithm thus gives a robust segmentation of the spinal canal on CT images. The method can be extended to other structures, although it remains to be shown that chamfer matching is sufficiently robust for the delineation of soft-tissue structures surrounded by soft tissue [13].

Yongjian Yu at.al (2004) presented a technique for semiautomated segmentation of human prostates using suprapubic ultrasound (US) images. A speckle reducing anisotropic diffusion (SRAD) is applied to enhance the images and the instantaneous coefficient of variation (ICOV) is utilized for edge detection. Segmentation is accomplished via a parametric active contour model in a polar coordinate system that is tailored to the application. The algorithm initially approximates the prostate boundary in two stages. First a primary contour is detected using an elliptical model, followed by a primary contour optimization using an area-weighted mean-difference binary flow geometric snake model. The algorithm was assessed by comparing the computer-derived contours with contours produced manually by three sonographers. The proposed method has application in radiation therapy planning and delivery, as well as in automated volume measurements for ultrasonic diagnosis. The average root mean square discrepancy between computed and manual outlines is less than the inter-observer variability. Furthermore, 76% of the computer-outlined contour is less than 1 σ manual outline variance away from "true" boundary of prostate. He concluded that the methods developed herein possess acceptable agreement with manually contoured prostate boundaries and that they are potentially valuable tools for radiotherapy treatment planning and verification [14].

Jun Xie et.al (2005) presented a novel texture and shape priors based method for kidney segmentation in ultrasound (US) images. Texture features are extracted by applying a bank of Gabor filters on test images through a two-sided convolution strategy. The texture model is constructed via estimating the parameters of a set of mixtures of half-planed Gaussians using the expectation-maximization method. Through this texture model, the texture similarities of areas around the segmenting curve were measured in the inside and outside regions, respectively. An iterative segmentation framework is presented to combine the texture measures into the parametric shape. Segmentation is implemented by calculating the parameters of the shape model to minimize a novel energy function. The goal of this energy function is to partition the test image into two regions, the inside one with high texture similarity and low texture variance, and the outside one with high texture variance. The effectiveness of this method is demonstrated through experimental results on both natural images and US data compared with other

image segmentation methods and manual segmentation. The proposed method is evaluated via experiments on both natural images and US images compared with manual raters and other image segmentation methods. The experiments on the maple leaf dataset showed the valid and efficiency of the proposed segmentation framework. Additionally, the experimental results on the medical US data are promising and showed that the approach can segment kidney in US images accurately and efficiently. The initial segmenting curves were positioned manually. Ideally a fully automated technique would be developed such that the prior model can be initialized on the test medical image in some sense optimal. However, it is a challenging perspective because it is hard to define what is optimal and the speckle patterns in US images are too complex [15].

Barbara Podda at.al (2005) presented a textural feature analysis applied to a medical image segmentation problem where other methods fail, i.e. the localization of thrombotic tissue in the aorta. This problem is extremely relevant because many clinical applications are being developed for the computer assisted, image driven planning of vascular intervention, but standard segmentation techniques based on edges or gray level thresholding are not able to differentiate thrombus from surrounding tissues like vena, pancreas having similar HU average and noisy patterns. A deep analysis of the texture segmentation approaches used for CT scans, and on experimental tests performed to find out textural features that better discriminate between thrombus and other tissues [16].

Esmeraldo dos SANTOS FILHO (2005) proposed a system for luminal contour segmentation in intravascular ultrasound images is proposed. Moment-based texture features are used for clustering of the pixels in the input image. After the clustering, morphological smoothing and a boundary detection process are applied and the final image is obtained. The proposed method was applied to 15 images from different patients, and a correlation coefficient of 0.86 was obtained between the areas of lumen automatically and manually defined. The author finally concluded the Moment-based texture features together with the radial feature are powerful tools for identification of the lumen region in intravascular ultrasound images. Morphological filtering was useful for improving the segmentation results. The moment based texture features together with radial distance were feasible components for a feature vector in IVUS image

segmentation when the aim is to find the luminal contour. However, some errors still occurred in the regions with shadows. The process was improved when a morphological smoothing filtering was carried out after the clustering and before the boundary detection process. Tests performed with 15 images from different patients resulted in a correlation coefficient of 0.86 between the lumen areas automatically detected and the lumen areas manually detected [17].

Springer Berlin (2005) proposed an approach for segmentation of ultrasound images using features extracted by orthogonal wavelet transforms that could be used in an interactive system. These features were the training data for the K-means clustering algorithm and the Bayes classifier. The result of classification was improved by using neighborhood information [18].

S. S. Mohamed et.al (2005) focused on extracting and analysing prostate texture features from trans-rectal ultrasound (TRUS) images for tissue characterization. One of the principal contributions of this investigation is the use of the information of the images' frequency domain features and spatial domain features to attain a more accurate diagnosis. Each image is divided into regions of interest (ROIs) by the Gabor multi-resolution analysis, a crucial stage, in which segmentation is achieved according to the frequency response of the image pixels. The pixels with a similar response to the same filter are grouped to form one ROI. Next, from each ROI two different statistical feature sets were constructed; the first set included four grey level dependence matrix (GLDM) features and the second set consisted of five grey level difference vector (GLDV) features. These constructed feature sets were then ranked by the mutual information feature selection (MIFS) algorithm. Here, the features that provided the maximum mutual information of each feature and class (cancerous and non-cancerous) and the minimum mutual information of the selected features were chosen, yeilding a reduced feature subset. The two constructed feature sets, GLDM and GLDV, as well as the reduced feature subset, were examined in terms of three different classifiers: the condensed k-nearest neighbour (CNN), the decision tree (DT) and the support vector machine (SVM). The accuracy classification results range from 87.5% to 93.75%, where the performance of the SVM and that of the DT are significantly better than the performance of the CNN.

This technique could be used as a support for the existing technologies for prostate cancer diagnosis and as a result aiding biopsy planning. The key advantage of the proposed algorithm is the application of multi-resolution texture segmentation for ROI identification, which leads to substantial time saving either by assisting the radiologist or by eliminating the need for whole image analysis [19].

Bassel Abou Merhy et.al (2005) presented a novel method for the segmentation of probabilistic two-dimensional occupancy maps, based on the analysis of their texture characteristics. The texture is represented by means of a double distribution of "Local Binary Pattern" and "Contrast". The logarithmic likelihood ratio, G-statistic, is used to measure the degree of similarity between different regions; this pseudo metric measure compares LBP/C distributions linked to different segments. The innovative algorithm is used to segment the probabilistic images in regions that characterize the space according to the certainty of its occupancy level. For a better interaction between an autonomous system and its environment, the segmentation scheme is also able to differentiate between objects present in the scene by analyzing the proximity between occupied segments. Along with experimental results, a comparison with other algorithms is provided in order to demonstrate the efficiency of the proposed approach. The new method proved to be effective and efficient in the case of probabilistic images constructed by means of a laser range sensor. Since the probabilistic environment is characterized by areas with relatively uniform texture, regions can be linked to create segments having similar occupancy level. This work provides a strong basis for our research on robot guidance from probabilistic models. Segmented probabilistic maps are now being used to optimize mobile platforms navigation in uncertain environments. This approach is also being extended for the segmentation of three-dimensional probabilistic environment models [20].

Mohsen Ghazel et.al (2006) proposed a reliable segmentation of multiple sclerosis lesions in magnetic resonance brain imaging for at least three types of practical applications: pharmaceutical trials, decision making for drug treatment or surgery, and patient follow-up. However, manual segmentation is hard to reproduce and can be time consuming in the presence of large volumes of MRI data. Automated segmentation methods are significantly faster and yield reproducible results. However, these automated methods

generally produce segmentation results that agree only partially with the ground truth segmentation provided by the experts.. In this paper, a semi-automated MS lesion detection system is proposed that combines the knowledge of the expert with the computational capacity to produce faster and more reliable MS segmentation results. In particular, the user selects coarse regions of interest (ROI's) that may potentially contain MS lesions. Then any MS lesions within the provided ROI's are then detected and segmented based on texture analysis. The method is applied on real MRI data and the results are qualitatively compared to a ground truth, which is manually segmented by a human expert. A semi-automated MS lesion detection and segmentation method based on texture analysis is presented. The method is based on performing texture analysis of prescribed ROI's provided by the user in order to select the most significant texture features that are capable of discriminating between the MS lesions and the healthy white matter tissues. These features are then used to classify the pixels into one of two classes - lesion or healthy tissue - and segment the MS lesions [21].

Constantino Carlos et.al (2007) presented a multiresolution volumetric texture segmentation (M-VTS) algorithm. The method extracts textural measurements from the Fourier domain of the data via subband filtering using an orientation. The most discriminant measurements and producing a compact feature space is selected. An oct tree is built of the multivariate features space and a chosen level at a lower spatial resolution is first classified. The classified voxel labels are then projected to lower levels of the tree where a boundary refinement procedure is performed with a three-dimensional (3-D) equivalent of butterfly filters. The algorithm was tested with 3-D artificial data and three magnetic resonance imaging sets of human knees with encouraging results. The regions segmented from the knees correspond to anatomical structures that can be used as a starting point for other measurements such as cartilage extraction. A multiresolution algorithm based on Fourier domain filtering was presented for the classification of texture volumes. Textural measurements were extracted in 3-D data by sub-band filtering with an Orientation Pyramid tessellation. Some of the measurements were selected to form a new feature space. A multiresolution algorithm was shown to improve the classification of these feature spaces: OTs was formed with the features. Once the classification was performed at a higher level of the tree, the class and boundary conditions of the elements

were then propagated down. A boundary refinement method with pyramidal, volumetric BFs is performed to regain spatial resolution. In the case of MRI, the effects of inhomogeneities artifacts were addressed [22].

Jesus Cerquides et.al (2007) introduced a machine learning approach into the process of direct volume rendering of biomedical high-resolution 3D images. In this paper, a learning pipeline process is proposed that generated the classification function within the optical property function that was used for rendering. Briefly, this pipeline started with a data acquisition and selection task, followed by a feature extraction process, to be ended with sequence of supervised learning steps. Learning comprises Gentle Boost and CRF (Conditional Random Fields) classifiers. The process is evaluated in terms of accuracy and overlap matrices and then increase in performance is measured along the whole pipeline process. Empirical results confirm that, even though the classification of high-resolution computerized tomography volume data poses a challenging problem for single-run classifiers, it was significantly improved by subsequent learning steps and refinements [23].

Rushin Shojaii et.al (2007) proposed a method that diagnosed several lung diseases are diagnosed based, texture segmentation which is an essential part of the most Computer Aided Diagnosis (CAD) systems. In this paper, a novel composite method is emphasized to segment the abnormality in lung tissue in pediatric CT images. The proposed approach is based on wavelet transform and intensity similarities. Honeycomb texture in lung tissue is focused. After segmenting lung regions, Wavelet Transform is applied to decompose the image. The vertical subimage of lung is thresholded to extract high resolution areas. Then the regions with low pixel intensities are kept and grown to segment the honeycomb regions. The proposed method has been tested on 91 pediatric chest CT images containing healthy and unhealthy lung images. They proposed approach can be further improved to detect all possible abnormalities with different types of textures in lung tissue. Multilevel thresholding can be utilized to separate different patterns with different resolutions. Automatic lung disease quantification is another field of research which is done on segmented abnormal region in CT images. It can also be

used to monitor the healing process or the improvement of the disease. Optimization methods can also be utilized to increase the specificity [24].

Dana Cobzas et.al (2007) proposed a variational brain tumor segmentation algorithm that extended current approaches from texture segmentation by using a high dimensional feature set calculated from MRI data and registered atlases. Using manually segmented data a statistical model for tumor and normal tissue is p[resented and showed that using a conditional model to discriminate between normal and abnormal regions significantly improves the segmentation results compared to traditional generative models. Validation is performed by testing the method on several cancer patient MRI scans. A variational method for brain tumor segmentation is shown. Existing region-based variational segmentation methods based on texture features are not suited for tumor segmentation as they are not discriminative enough when the appearance of tumor and normal tissue overlap. Using priors of the appearance of anatomical structures in the normal brain in the form of templates and atlases, they defined a set of multidimensional features and used them to calculate statistics for 'tumor' and 'normal brain' area from labeled MRI data. A discriminatively-trained conditional model based on Logistic Regression gives better results than traditional generative models [25].

Jiahui Wang et.al (2007) developed a novel automated method for accurate segmentation of nodules in three-dimensional (3D) CT. First, a volume of interest (VOI) was determined at the location of a nodule. To simplify nodule segmentation, the 3D VOI was transformed into a two-dimensional (2D) image by use of a key “spiralscanning” technique, in which a number of radial lines originating from the center of the VOI spirally scanned the VOI from the “north pole” to the “south pole.” The voxels scanned by the radial lines provided a transformed 2D image. Because the surface of a nodule in the 3D image became a curve in the transformed 2D image, the spiral-scanning technique considerably simplified the segmentation method and enabled reliable segmentation results to be obtained. A dynamic programming technique was employed to delineate the “optimal” outline of a nodule in the 2D image, which corresponded to the surface of the nodule in the 3D image. The optimal outline was then transformed back into 3D image space to provide the surface of the nodule. An overlap between nodule regions provided

by computer and by the radiologists was employed as a performance metric for evaluating the segmentation method. The segmentation method provided relatively reliable results for pulmonary nodule segmentation and would be useful for lung cancer quantification, detection, and diagnosis. A key contribution of their segmentation method is the transformation of 3D images to 2D image space by use of a spiral scanning technique, which considerably simplifies the segmentation scheme and improves its performance. A unique 3D reconstruction method was developed for transforming the segmented optimal outline of a nodule in the transformed 2D image into a solid volume of the nodule in 3D image space. The experiments on the LIDC database demonstrated that the segmentation method provided relatively robust and accurate results for the segmentation of pulmonary nodules, and would be useful for the quantification, detection, and diagnosis of lung cancer [26]

Claude et.al (2008) tried to perform a reliable segmentation without such prior information, starting from an upper bound of the number of texture classes. At a low resolution level, the image model assumes an autoregressive (AR) structure for the class-conditional random field. The SEM procedure is then applied to the set of AR features, yielding an estimate of the true number of texture classes, as well as estimates of the class-conditional AR parameters, and a coarse pre-segmentation. In a final stage, a regularization process is introduced for region formation by the way of a simple pairwise interaction model, and a finer segmentation is obtained through the maximization of posterior marginal. Some experimental results obtained by applying this method to synthetic textured and remote sensing images were presented [27].

Li Ma (2008) proposed an approach for texture segmentation that lies in the integrating statistical features derived from directional FD and gray-level statistics in a given preset window. The proposed method consists of three steps: firstly the fractal values at eight different directions are calculated; the statistical features on the directional FD are then extracted and combined with gray-level statistics. The experiments taken from both textile and medical images showed significantly effective of the proposed scheme A feature extraction method is developed for the texture image classification. The novelty in the paper lies in the integrating fractal dimension (FD) related features and their

corresponding statistics, plus grey level statistics for texture segmentation. The experiments showed that the proposed method is significantly effective both for textile images with many texture classes and medical images. As for the further improvements concerned, thicker edges appearing among different texture regions need to be refined. That may relate to the size of window chosen for calculating directional fractal values. The smaller size would produce thinner edges so we need to do further experimental study with changed window sizes and applying post-processing to improve the region boundaries [28].

CHAPTER 3
BIOMEDICAL IMAGING

3.1 INTRODUCTION

Magnetic resonance imaging is a relatively new technology. The first MR image was published in 1973 and the first study performed on a human took place on July 3, 1977. By comparison, the first human X-ray image was taken in 1895. Magnetic resonance imaging was developed from knowledge gained in the study of nuclear magnetic resonance. In its early years the technique was referred to as nuclear magnetic resonance imaging (NMRI).

However, as the word nuclear was associated in the public mind with ionizing radiation exposure it is generally now referred to simply as MRI. Scientists still use the term NMRI when discussing non-medical devices operating on the same principles. The term Magnetic Resonance Tomography (MRT) is also sometimes used. One of the contributors to modern MRI, which was later named the technique zeugmatography. The term referred to the interaction between the static, radio frequency, and gradient magnetic fields necessary to create an image, but this term was not adopted.

3.2 MAGNETIC RESONANCE IMAGING

Magnetic Resonance Imaging (MRI), or nuclear magnetic resonance imaging (NMRI), is primarily a medical imaging technique most commonly used in radiology to visualize the internal structure and function of the body. MRI provides much greater contrast between the different soft tissues of the body than computed tomography (CT) does, making it especially useful in neurological (brain), musculoskeletal, cardiovascular, and oncological (cancer) imaging.

Unlike CT, it uses no ionizing radiation, but uses a powerful magnetic field to align the nuclear magnetization of (usually) hydrogen atoms in water in the body.

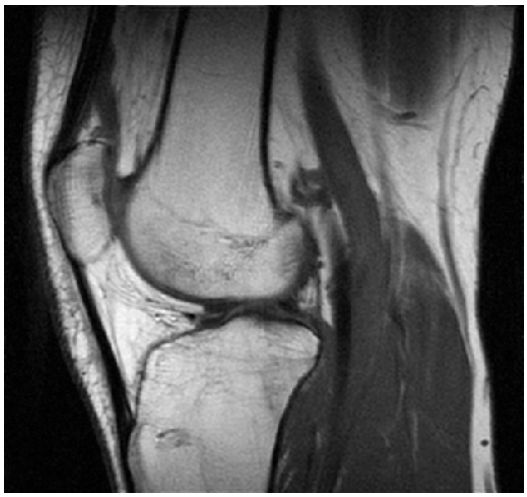

Figure 3.1: Sagittal MR image of the knee

Radio frequency (RF) fields are used to systematically alter the alignment of this magnetization, causing the hydrogen nuclei to produce a rotating magnetic field detectable by the scanner. This signal can be manipulated by additional magnetic fields to build up enough information to construct an image of the body.

3.3 WORKING OF MRI

Figure 3.2: Modern 3 tesla clinical MRI scanner

The body is mainly composed of water molecules which each contain two hydrogen nuclei or protons. When a person goes inside the powerful magnetic field of the scanner these protons align with the direction of the field. A second radio frequency electromagnetic field is then briefly turned on causing the protons to absorb some of its energy. When this field is turned off the protons release this energy at a radio frequency which can be detected by the scanner. The position of protons in the body can be determined by applying additional magnetic fields during the scan which allows an image of the body to be built up. These are created by turning gradients coils on and off which creates the knocking sounds heard during an MR scan.

Diseased tissue, such as tumors, can be detected because the protons in different tissues return to their equilibrium state at different rates. By changing the parameters on the scanner this effect is used to create contrast between different types of body tissue. Contrast agents may be injected intravenously to enhance the appearance of blood vessels, tumors or inflammation. Contrast agents may also be directly injected into a joint in the case of arthrograms, MR images of joints. Unlike CT, scanning MRI uses no ionizing radiation and is generally a very safe procedure. Patients with some metal implants, cochlear implants, and cardiac pacemakers are prevented from having an MRI scan due to effects of the strong magnetic field and powerful radio frequency pulses. MRI is used to image every part of the body, and is particularly useful for neurological conditions, for disorders of the muscles and joints, for evaluating tumors, and for showing abnormalities in the heart and blood vessels.

3.4 PHYSICS PRINCIPLES

Subatomic particles such as protons have the quantum mechanical property of spin. Certain nuclei such as ^{1}H (protons), ^{2}H, ^{3}He, ^{23}Na or ^{31}P, have a non–zero spin and therefore a magnetic moment. In the case of the so-called spin-1/2 nuclei, such as ^{1}H, there are two spin states, sometimes referred to as "up" and "down". Nuclei such as ^{12}C have no unpaired neutrons or protons, and no net spin; however, the isotope ^{13}C (referred to as "carbon 13") does.

When these spins are placed in a strong external magnetic field they process around an axis along the direction of the field. Protons align in two energy "eigenstates" (the

"Zeeman effect"): one low-energy and one high-energy, which are separated by a certain splitting energy.

3.5 IMAGING

A number of schemes have been devised for combining field gradients and radio frequency excitation to create an image. One involves 2D or 3D reconstruction from projections, much as in Computed Tomography. Others involve building the image point-by-point or line-by-line. One even uses gradients in the RF field rather than the static field. Although each of these schemes is occasionally used in specialist applications, the majority of MR Images today are created either by the Two-Dimensional Fourier Transform (2DFT) technique with slice selection, or by the Three-Dimensional Fourier Transform (3DFT) technique. Another name for 2DFT is spin-warp. What follows here is a description of the 2DFT technique with slice selection.

Slice selection is achieved by applying a magnetic gradient in addition to the external magnetic field during the radio frequency pulse. Only one plane within the object will have protons that are on–resonance and contribute to the signal. A real image can be considered as being composed of a number of spatial frequencies at different orientations. A two–dimensional Fourier transformation of a real image will express these waves as a matrix of spatial frequencies known as k–space. Low spatial frequencies are represented at the center of k–space and high spatial frequencies at the periphery. Frequency and phase encoding are used to measure the amplitudes of a range of spatial frequencies within the object being imaged.

The frequency encoding gradient is applied during readout of the signal and is orthogonal to the slice selection gradient. During application of the gradient the frequency differences in the readout direction progressively change. At the midpoint of the readout these differences are small and the low spatial frequencies in the image are sampled filling the center of k-space. Higher spatial frequencies will be sampled towards the beginning and end of the readout filling the periphery of k-space.

Phase encoding is applied in the remaining orthogonal plane and uses the same principle of sampling the object for different spatial frequencies. However, it is applied for a brief

period before the readout and the strength of the gradient is changed incrementally between each radio frequency pulse. For each phase encoding step a line of k–space is filled. Either a spin echo or a gradient echo can be used to refocus the magnetisation. The 3DFT technique is rather similar except that there is no slice selection and phase-encoding is performed in two separate directions.

Another scheme which is sometimes used, especially in brain scanning or where images are needed very rapidly, is called echo-planar imaging (EPI): In this case, each RF excitation is followed by a train of gradient echoes with different spatial encoding.

3.6 IMAGE CONTRAST AND CONTRAST ENHANCEMENT

Image contrast is created by differences in the strength of the NMR signal recovered from different locations within the sample. This depends upon the relative density of excited nuclei (usually water protons), on differences in relaxation times (T_1, T_2 and T_2 *) of those nuclei after the pulse sequence, and often on other parameters discussed under specialized MR scans. Contrast in most MR images is actually a mixture of all these effects, but careful design of the imaging pulse sequence allows one contrast mechanism to be emphasized while the others are minimized.

The ability to choose different contrast mechanisms gives MRI tremendous flexibility. In the brain, T_1-weighting causes the nerve connections of white matter to appear white, and the congregations of neurons of gray matter to appear gray, while cerebrospinal fluid (CSF) appears dark. The contrast of white matter, gray matter and cerebrospinal fluid is reversed using T_2 or T_2 * imaging, whereas proton-density-weighted imaging provides little contrast in healthy subjects. Additionally, functional parameters such as cerebral blood flow (CBF), cerebral blood volume (CBV) or blood oxygenation can affect T_1, T_2 and T_2 * and so can be encoded with suitable pulse sequences.

In some situations it is not possible to generate enough image contrast to adequately show the anatomy or pathology of interest by adjusting the imaging parameters alone, in which case a contrast agent may be administered. This can be as simple as water, taken orally, for imaging the stomach and small bowel. However, most contrast agents used in MRI are selected for their specific magnetic properties. Most commonly, a paramagnetic

contrast agent (usually a gadolinium compound is given. Gadolinium-enhanced tissues and fluids appear extremely bright on T1-weighted images. This provides high sensitivity for detection of vascular tissues (*e.g.*, tumors) and permits assessment of brain perfusion (*e.g.*, in stroke). There have been concerns raised recently regarding the toxicity of gadolinium-based contrast agents and their impact on persons with impaired kidney function. The American College of Radiology released screening criteria for patients intended to be given gadolinium-based contrast agents to identify potential risk factors for negative reactions. Special actions may be taken, such as hemodialysis following a contrast MRI scan for renally-impaired patients.

More recently, superparamagnetic contrast agents, *e.g.*, iron oxide nanoparticles have become available. These agents appear very dark on T2*-weighted images and may be used for liver imaging, as normal liver tissue retains the agent, but abnormal areas (*e.g.*, scars, tumors) do not. They can also be taken orally, to improve visualization of the gastrointestinal tract, and to prevent water in the gastrointestinal tract from obscuring other organs (*e.g.*, the pancreas). Diamagnetic agents such as barium sulfate have also been studied for potential use in the gastrointestinal tract, but are less frequently used.

3.7 SCANNER CONSTRUCTION AND OPERATION

The three systems described above form the major components of an MRI scanner:

Magnetic Resonance Imaging (MRI), or nuclear magnetic resonance imaging (NMRI), is primarily a medical imaging technique most commonly used in radiology to visualize the internal structure and function of the body. MRI provides much greater contrast between the different soft tissues of the body than computed tomography (CT) does, making it especially useful in neurological (brain), musculoskeletal, cardiovascular, and oncological (cancer) imaging.

1. A static magnetic field,
2. A RF transmitter and receiver, and
3. 3 orthogonal, controllable magnetic gradients.

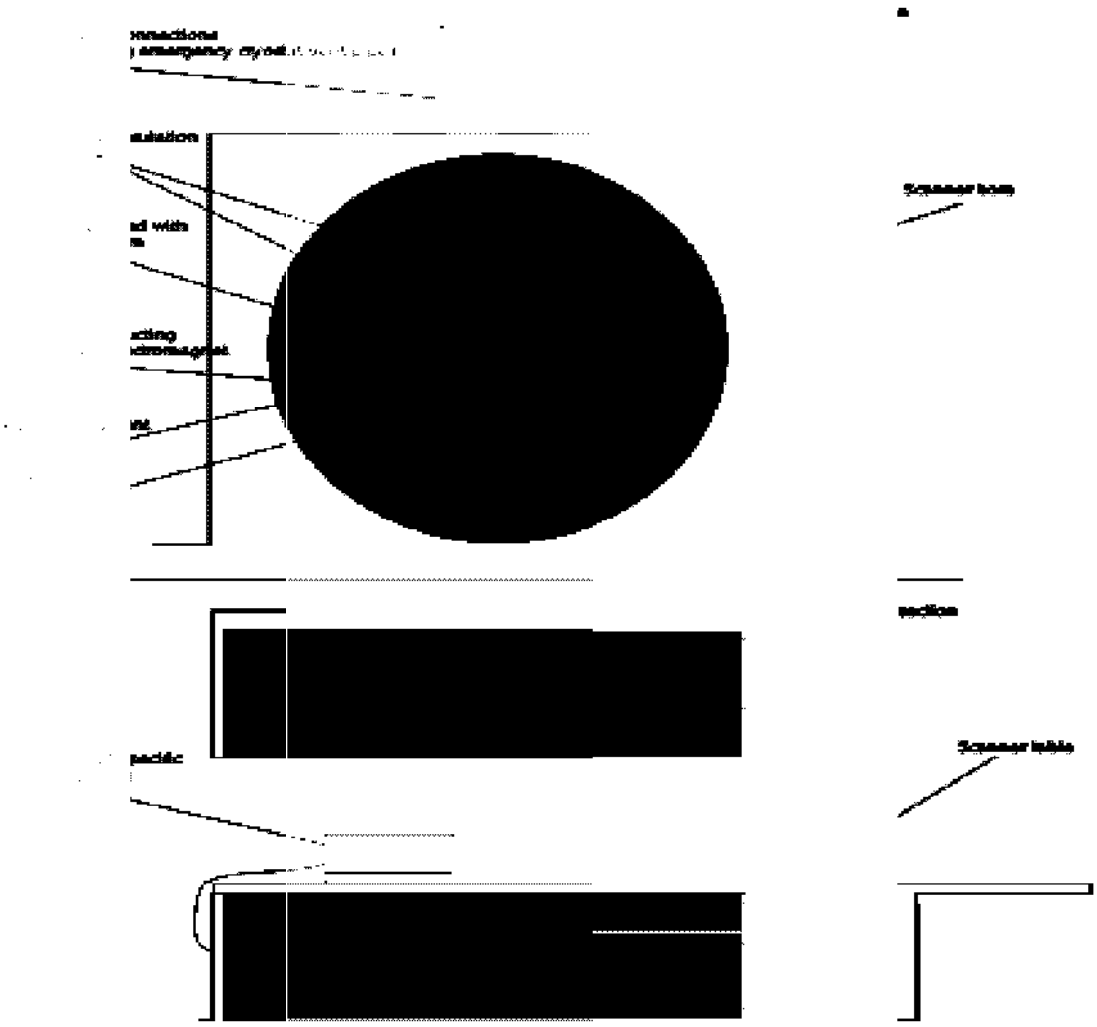

Figure 3.3 Schematic of construction of a cylindrical superconducting MR scanner

3.8 APPLICATIONS

In clinical practice, MRI is used to distinguish pathologic tissue (such as a brain tumor) from normal tissue. One advantage of an MRI scan is that it is harmless to the patient. It uses strong magnetic fields and non-ionizing radiation in the radio frequency range.

Compare this to CT scans and traditional X-rays which involve doses of ionizing radiation and may increase the risk of malignancy, especially in a fetus.

While CT provides good spatial resolution (the ability to distinguish two structures an arbitrarily small distance from each other as separate), MRI provides comparable resolution with far better contrast resolution (the ability to distinguish the differences between two arbitrarily similar but not identical tissues). The basis of this ability is the complex library of pulse sequences that the modern medical MRI scanner includes, each of which is optimized to provide image contrast based on the chemical sensitivity of MRI.

For example, with particular values of the echo time (TE) and the *repetition time* (TR), which are basic parameters of image acquisition, a sequence will take on the property of T2-weighting. On a T2-weighted scan, water- and fluid-containing tissues are bright (most modern T2 sequences are actually *fast T2* sequences) and fat-containing tissues are dark. The reverse is true for T1-weighted images. Damaged tissue tends to develop edema, which makes a T2-weighted sequence sensitive for pathology, and generally able to distinguish pathologic tissue from normal tissue.

With the addition of an additional radio frequency pulse and additional manipulation of the magnetic gradients, a T2-weighted sequence can be converted to a FLAIR sequence, in which free water is now dark, but edematous tissues remain bright. This sequence in particular is currently the most sensitive way to evaluate the brain for demyelinating diseases, such as multiple sclerosis. The typical MRI examination consists of 5-20 sequences, each of which are chosen to provide a particular type of information about the subject tissues. This information is then synthesized by the interpreting physician.

3.9 BASIC MRI SCANS

Comparison of Different Types of MR Contrast

1. T1 Weighting 2. T2 Weighting

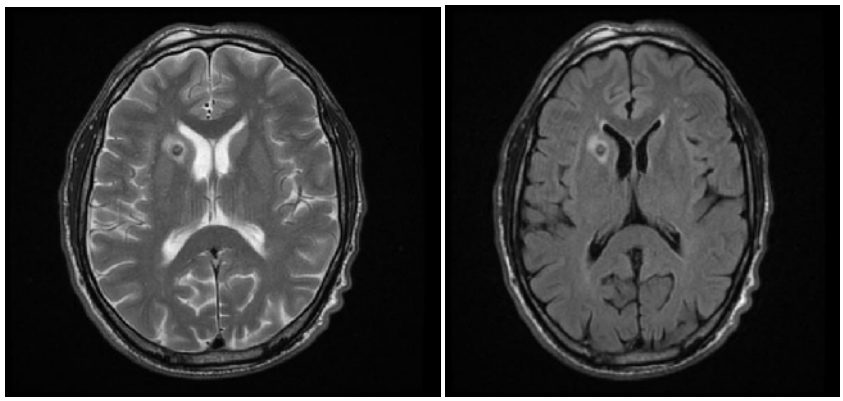

(a) (b)

3. Flair 4. T2* Weighting

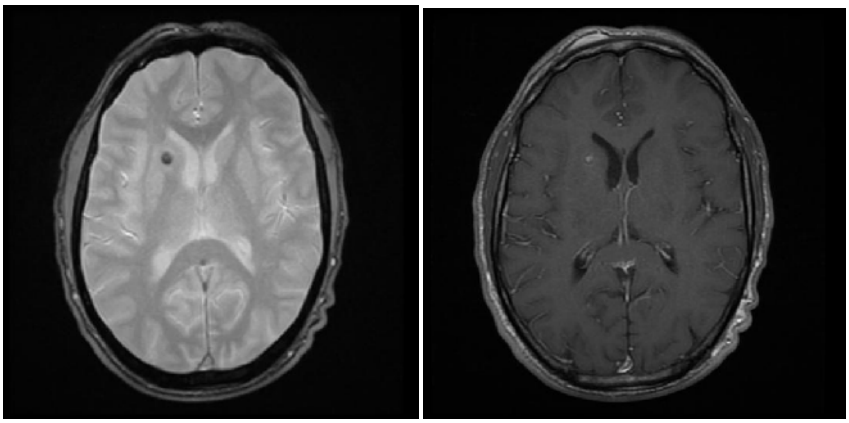

(c) (d)

Figure 3.4: Different types of MR contrast

3.9.1 T1 WEIGHTED MRI

T1 weighted scans use a gradient echo (GRE) sequence, with short TE and short TR. This is one of the basic types of MR contrast and is a commonly run clinical scan. The T1 weighting can be increased (improving contrast) with the use of an inversion pulse as in an MP-RAGE sequence. Due to the short repetition time (TR) this scan can be run very fast allowing the collection of high resolution 3D datasets. A T1 reducing gadolinium contrast agent is also commonly used with a T1 scan being collected before and after administration of contrast agent to compare the difference. In the brain T1 weighted scans provide good gray matter/white matter contrast.

3.9.2 T2 WEIGHTED MRI

T2 weighted scans use a spin echo (SE) sequence, with long TE and long TR. They have long been the clinical workhorse as the spin echo sequence is less susceptible to inhomogeneities in the magnetic field. They are particularly well suited to edema as they are sensitive to water content (edema is characterized by increased water content).

3.9.3 T2* WEIGHTED MRI

T2* weighted scans use a gradient echo (GRE) sequence, with long TE and long TR. The gradient echo sequence used does not have the extra refocusing pulse used in spin echo so it is subject to additional losses above the normal T2 decay (referred to as T2'), these taken together are called T2*. This also makes it more prone to susceptibility losses at air/tissue boundaries, but can increase contrast for certain types of tissue, such as venous blood.

3.9.4 SPIN DENSITY WEIGHTED MRI

Spin density, also called proton density, weighted scans try to have no contrast from either T2 or T1 decay, the only signal change coming from differences in the amount of available spins. It uses a gradient echo sequence, with short TE and long TR.

3.10 SPECIALIZED MRI SCANS

Diffused MRI scan is the specialized MRI scan which measures the water molecules diffusion.

3.10.1 DIFFUSION MRI

Diffusion MRI measures the diffusion of water molecules in biological tissues. In an isotropic medium (inside a glass of water for example) water molecules naturally move randomly according to Brownian motion. In biological tissues however, the diffusion may be anisotropic. For example a molecule inside the axon of a neuron has a low probability of crossing the myelin membrane. Therefore the molecule will move principally along the axis of the neural fiber. If we know that molecules in a particular voxel diffuse principally in one direction we can make the assumption that the majority of the fibers in this area are going parallel to that direction.

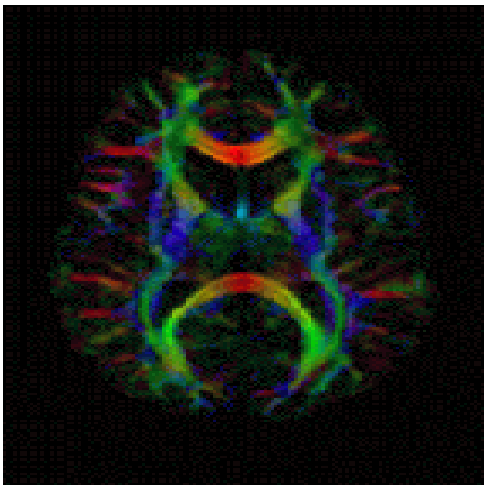

Figure 3.5: Diffusion MRI

The recent development of diffusion tensor imaging (DTI) enables diffusion to be measured in multiple directions and the fractional anisotropy in each direction to be calculated for each voxel. This enables researchers to make brain maps of fiber directions to examine the connectivity of different regions in the brain (using tractography) or to examine areas of neural degeneration and demyelination in diseases like Multiple Sclerosis.

Another application of diffusion MRI is diffusion-weighted imaging (DWI). Following an ischemic stroke, DWI is highly sensitive to the changes occurring in the lesion. It is speculated that increases in restriction (barriers) to water diffusion, as a result of cytotoxic edema (cellular swelling), is responsible for the increase in signal on a DWI scan. The DWI enhancement appears within 5-10 minutes of the onset of stroke symptoms (as compared with computed tomography, which often does not detect changes of acute infarct for up to 4–6 hours) and remains for up to two weeks. Coupled with imaging of cerebral perfusion, researchers can highlight regions of "perfusion/diffusion mismatch" that may indicate regions capable of salvage by reperfusion therapy.

Like many other specialized applications, this technique is usually coupled with a fast image acquisition sequence, such as echo planar imaging sequence.

3.11 MAGNETIC RESONANCE ANGIOGRAPHY

It is used to generate pictures of the arteries in order to evaluate them for stenosis (abnormal narrowing) or aneurysms (vessel wall dilatations, at risk of rupture). MRA is often used to evaluate the arteries of the neck and brain, the thoracic and abdominal aorta, the renal arteries, and the legs (called a "run-off").

Figure 3.6: Magnetic Resonance Angiography

A variety of techniques can be used to generate the pictures, such as administration of a paramagnetic contrast agent (gadolinium) or using a technique known as "flow-related enhancement" (e.g. 2D and 3D time-of-flight sequences), where most of the signal on an image is due to blood which has recently moved into that plane, see also FLASH MRI.

Techniques involving phase accumulation (known as phase contrast angiography) can also be used to generate flow velocity maps easily and accurately. Magnetic resonance venography (MRV) is a similar procedure that is used to image veins. In this method the tissue is now excited inferiorly while signal is gathered in the plane immediately superior to the excitation plane, and thus imaging the venous blood which has recently moved from the excited plane.

3.12 ADVANTAGES OF MRI

1. It can noninvasively record brain signals (of humans and other animals) without risks of radiation inherent in other scanning methods, such as CT or PET scans.
2. It can record on a spatial resolution of less than 1 millimeter, although resolution in the region of 3-6 millimeters is more typical, but with poor temporal resolution (on the order of seconds) compared with techniques such as EEG. However, this is mainly because of the hemodynamic phenomena being measured, not because of the technique. EEG measures electrical/neural activity while fMRI measures blood activity, which has a slower response. The MRI equipment used for fMRI can be used for high temporal resolution, if one measures different phenomena.

3.13 DISADVANTAGES OF fMRI

1. The BOLD signal is only an indirect measure of neural activity, and is therefore susceptible to influence by non-neural changes in the body.
2. BOLD signals are most strongly associated with the input to a given area rather than with the output. It is therefore possible (although unlikely) that a BOLD signal could be present in a given area even if there is no single unit activity.
3. Different brain areas may have different thermodynamic responses, which would not be accurately reflected by the simplest version of the general linear model often used to filter fMRI time signals.
4. The temporal response of the blood supply, which is the basis of fMRI, is slow relative to the electrical signals that define neuronal communication. To alleviate this problem, some research groups are attempting to combine fMRI signals that have relatively high spatial resolution with signals recorded with other techniques, electroencephalography (EEG) or magneto encephalography (MEG), which have higher temporal resolution but worse spatial resolution.
5. fMRI has often been used to show activation localized to specific regions, thus minimizing the distributed nature of processing in neural networks. Several recent multivariate statistical techniques work around this issue by characterizing interactions between "active" regions found via traditional univariate techniques.

6. fMRI has poor signal-to-noise ratio, at least in comparison to many electrophysiological techniques. This necessitates extensive post-processing and published fMRI results are often heavily averaged over time and smoothed across space using one of several software packages.

3.14 CONCLUSION

MRI is a medical imaging technique most commonly used in radiology to visualize the internal structure and function of the body. It provides much greatest contrast between the different soft tissues of the body than computed tomography (CT) does, making it especially useful in neurological, musculoskeletal, cardiovascular, and oncological imaging. This technique can be used for other medical imaging also.

CHAPTER 4
TEXTURE ANALYSIS

4.1 INTRODUCTION

It is the process of algorithmically constructing a large digital image from a small digital sample image by taking advantage of its structural content. It is object of research to computer graphics and is used in many fields, amongst others digital image editing, 3D computer graphics and post-production of films.

4.2 TEXTURES

Texture is an ambiguous word and in the context of texture synthesis may have one of the following meanings:

1. In common speech, "texture" used as a synonym for "surface structure". Texture has been described by five different properties in the psychology of perception: coarseness, contrast, directionality, line-likeness and roughness.
2. In 3D computer graphics, a texture is a digital image applied to the surface of a three-dimensional model by texture mapping to give the model a more realistic appearance. Often, the image is a photograph of a "real" texture, such as wood grain.
3. In image processing, every digital image composed of repeated elements is called a texture.

Texture can be arranged along a spectrum going from stochastic to regular:

1. Stochastic textures. Texture images of stochastic textures look like noise: colour dots that are randomly scattered over the image, barely specified by the attributes minimum and maximum brightness and average colour. Many textures look like stochastic textures when viewed from a distance. An example of a stochastic texture is roughcast.
2. Structured textures. These textures look like somewhat regular patterns. An example of a structured texture is a stonewall or a floor tiled with paving stones.

Texture synthesis can be used to fill in holes in images, create large non-repetitive background images and expand small pictures.

4.3 INFORMATION EXTRACTION USING TEXTURE ANALYSIS

Texture analysis refers to a class of mathematical procedures and models that characterize the spatial variations within imagery as a means of extracting information. Texture is an areal construct that defines local spatial organization of spatially varying spectral values that is repeated in a region of larger spatial scale. Thus, the perception of texture is a function of spatial and radiometric scales. Mathematical procedures to characterize texture fall into four general categories, statistical, geometrical, model-based methods and signal processing methods and include Fourier transforms, convolution filters, co-occurrence matrix, spatial autocorrelation, fractals, etc. Because texture has so many different dimensions, there is no single method of texture representation that is adequate for a variety of textures. Here, we provide a brief description of a number of texture analysis techniques and some examples. Many terms will be unfamiliar to the reader and one is encouraged to seek other sources for more in depth discussion. Most image processing software packages that are commercially available today include several texture analysis tools. Few, however, make full use of these tools because of the difficulty interpreting results. Despite their potential value, textural measures have not been exploited in any formal way for routine monitoring of landscape change. Although, texture analysis has been used to classify remotely sensed images, its value is restricted within the limitations afforded by classification. The spatial variations in image values that constitute texture are generally due to some underlying physical variation in the landscape that alters the reflectivity or emissivity. Textural analysis techniques can be used to provide quantitative metrics that are highly sensitive to the underlying processes of change.

4.3.1 TECHNIQUES INVOLVED

A wide variety of techniques for describing image texture have been proposed. Four major categories for analysis techniques statistical, geometrical, model-based and signal processing.

4.3.1.1 STATISTICAL METHODS

Statistical methods analyze the spatial distribution of gray values by computing local features at each point in the image and deriving a set of statistics from the distributions of the local features. The reason behind that is the fact that the spatial distribution of gray values is one of the defining qualities of texture. Statistical methods can be classified into first-order (one pixel), second-order (two pixels) and higher-order (three or more pixels) statistics based on the number of pixels defining the local feature. The first-order statistics estimate properties like the average and variance of individual pixel values, ignoring the spatial interaction between image pixels, second- and higher-order statistics on the other hand estimate properties of two or more pixel values occurring at specific locations relative to each other. Co-occurrence features and gray level differences are the most widely used statistical methods, which inspired a variety of modifications later on including signed differences and the Local Binary Pattern (LBP) operator. LBP operator combines statistical and structural approaches to texture analysis by incorporating occurrence statistics of simple local microstructures. Autocorrelation function, which has been used for analyzing the regularity and coarseness of texture, and gray level run lengths are examples of other statistical approaches.

4.3.1.2 GEOMETRICAL METHODS

Geometrical methods try to describe the primitives and the rules governing their spatial organization by considering texture to be composed of texture primitives. The structure and organization of the primitives can be presented. An example of often-used primitive elements would be image edges. The desirable properties in defining local spatial neighborhoods and because the local spatial distributions of tokens are reflected in the shapes of the tessellations are some of the advantages of this method. Segmentation of textured images is one example of texture features based on Voronoi polygons (Figure 1). Gray level texture images and a number of synthetic textures have been successfully segmented with identical second-order statistics by this algorithm.

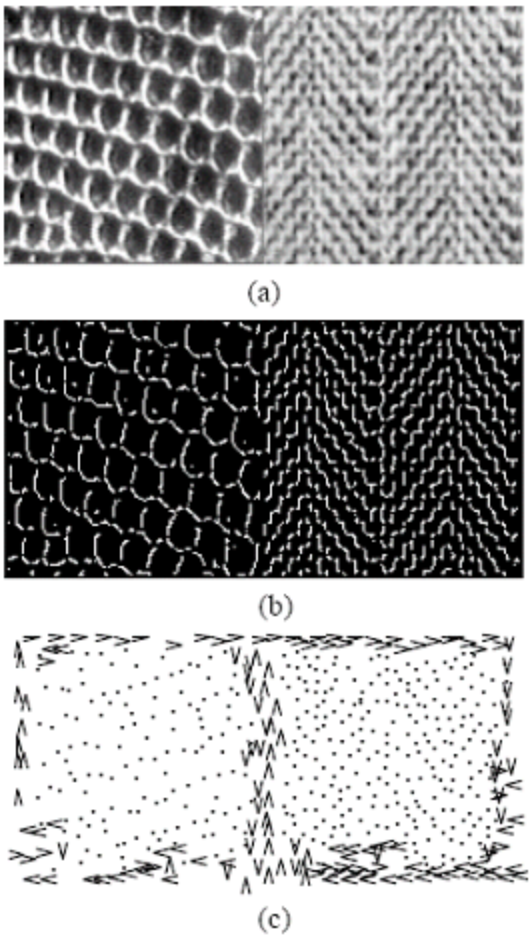

Figure 4.1: Texture segmentation
(a) An example texture pair (b) the peaks detected in the filtered image, and (c) the segmentation using the texture features

4.3.1.3 MODEL-BASED METHODS

Model based texture analysis methods are based on the construction of an image model that can be used not only to describe texture, but also to synthesize it. The model parameters capture the essential perceived qualities of texture. These methods hypothesize the underlying texture process, constructing a parametric generative model, which could have created the observed intensity. The intensity function is considered to be a combination of a function representing the known structural information on the image surface and an additive random noise sequence. Pixel-based models view an image as a collection of pixels, whereas region-based models regard an image as a set of subpatterns placed according to given rules. Region-based models are an example of random mosaic models, which tessellate the image into regions and assign gray levels to

the regions according to a specified probability density function. The facet model is a pixel-based model, which assumes no spatial interaction between neighboring pixels, and the observed intensity function is assumed to be the sum of a deterministic polynomial and additive noise. Random field models analyze spatial variations in two dimensions. Global random field models treat the entire image as a realization of a random field, whereas local random field models assume relationships of intensities in small neighborhoods. A Gibbs random field is a global model, where using cliques of neighboring pixels as the neighborhood system, a probability density function is assigned to the entire image. Markov random fields (MRFs) have been popular for modeling images because they are able to capture the local (spatial) contextual information in an image. These models assume that the intensity at each pixel in the image depends on the intensities of only the neighboring pixels. MRF models have been applied to various image processing applications, such as texture synthesis Model-based Methods

Model based texture analysis methods are based on the construction of an image model that can be used not only to describe texture, but also to synthesize it. The model parameters capture the essential perceived qualities of texture. These methods hypothesize the underlying texture process, constructing a parametric generative model, which could have created the observed intensity distribution. The intensity function is considered to be a combination of a function representing the known structural information on the image surface and an additive random noise sequence. Pixel-based models view an image as a collection of pixels, whereas region-based models regard an image as a set of subpatterns placed according to given rules. Region-based models are an example of random mosaic models, which tessellate the image into regions and assign gray levels to the regions according to a specified probability density function. The facet model is a pixel-based model, which assumes no spatial interaction between neighboring pixels, and the observed intensity function is assumed to be the sum of a deterministic polynomial and additive noise. Random field models analyze spatial variations in two dimensions.

Global random field models treat the entire image as a realization of a random field, whereas local random field models assume relationships of intensities in small

neighborhoods. A Gibbs random field is a global model, where using cliques of neighboring pixels as the neighborhood system, a probability density function is assigned to the entire image. Markov random fields (MRFs) have been popular for modeling images because they are able to capture the local (spatial) contextual information in an image. These models assume that the intensity at each pixel in the image depends on the intensities of only the neighboring pixels. MRF models have been applied to various image processing applications, such as texture synthesis, texture classification and; image segmentation, image restoration and image compression

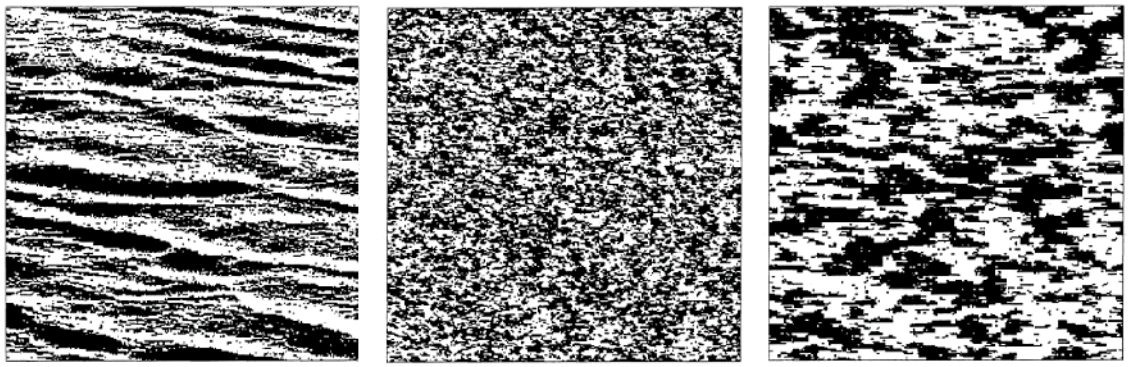

Figure 4.2: Example of water texture synthesis. (a) Original water texture, (b) The synthesized water texture with MRF modeling, (c) The synthesized water texture

4.4 ANALYZING THE TEXTURE OF AN IMAGE

Texture analysis refers to the characterization of regions in an image by their texture content. Texture analysis attempts to quantify intuitive qualities described by terms such as rough, smooth, silky, or bumpy as a function of the spatial variation in pixel intensities. In this sense, the roughness or bumpiness refers to variations in the intensity values, or gray levels.

Texture analysis is used in a variety of applications, including remote sensing, automated inspection, and medical image processing. Texture analysis can be used to find the texture boundaries, called texture segmentation. Texture analysis can be helpful when objects in an image are more characterized by their texture than by intensity, and traditional thresholding techniques cannot be used effectively.

4.5 USING TEXTURE FILTER FUNCTIONS

The following are the texture filter function that provides the textural properties of the image:

1. rangefilt : Calculates the local range of an image
2. stdfilt: Calculates the local standard deviation of an image.
3. entropyfilt: Calculates the local entropy of a grayscale image. Entropy is a statistical measure of randomness.
4. graycorps: Calculates the contrast, correlation, energy and homogeneity of a an image.

These statistics can characterize the texture of an image because they provide information about the local variability of the intensity values of pixels in an image. For example, in areas with smooth texture, the range of values in the neighborhood around a pixel will be a small value; in areas of rough texture, the range will be larger. Similarly, calculating the standard deviation of pixels in a neighborhood can indicate the degree of variability of pixel values in that region.

4.6 TEXTURE FILTER FUNCTIONS

The functions all operate in a similar way: they define a neighborhood around the pixel of interest, the statistic for that neighborhood is calculated, and that value as the value of the pixel of interest in the output image is used.

This example shows how the rangefilt function operates on a simple array.

```
A = [ 1 2 3 4 5; 6 7 8 9 10; 11 12 13 14 15; 16 17 18 19 20 ]        4.1
```

```
A =   1   2   3   4   5
      6   7   8   9  10                                              4.2
     11  12  13  14  15
     16  17  18  19  20
```

```
B = rangefilt(A)                                                     4.3
```

```
B =   6   7   7   7   6
     11  12  12  12  11                                              4.4
     11  12  12  12  11
      6   7   7   7   6
```

The following figure shows how the value of element B (2,4) was calculated from A(2,4). By default, the rangefilt function uses a 3-by-3.

4.7 DETERMINING PIXEL VALUES IN RANGE FILTERED OUTPUT IMAGE

The stdfilt and entropyfilt functions operate similarly, defining a neighborhood around the pixel of interest and calculating the statistic for the neighborhood to determine the pixel value in the output image. The stdfilt function calculates the standard deviation of all the values in the neighborhood.

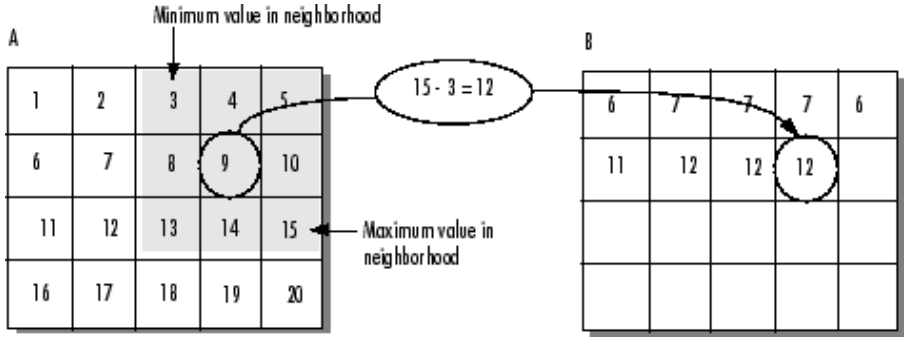

Figure 4.3: Determination pixel values in range filtered output image

The entropyfilt function calculates the entropy of the neighborhood and assigns that value to the output pixel. Note that, by default, the entropyfilt function defines a 9-by-9 neighborhood around the pixel of interest. To calculate the entropy of an entire image, use the entropy function.

4.8 EXAMPLE: USING THE TEXTURE FUNCTIONS

The following example illustrates how the texture filter functions can detect regions of texture in an image. In the figure, the background is smooth; there is very little variation in the gray-level values. In the foreground, the surface contours of the coins exhibit more texture. In this image, foreground pixels have more variability and thus higher range values. Range filtering makes the edges and contours of the coins more visible.

An example of using filtering functions

1. Read in the image and display it.

```
I = imread('eight.tif');                    4.5
imshow(I)                                   4.6
```

Figure 4.4: Original Image

2. Filter the image with the rangefilt function and display the results. Note how filtering highlights the edges range and surface contours of the coins.

```
K = rangefilt(I);                    4.7
figure, imshow(K)                    4.8
```

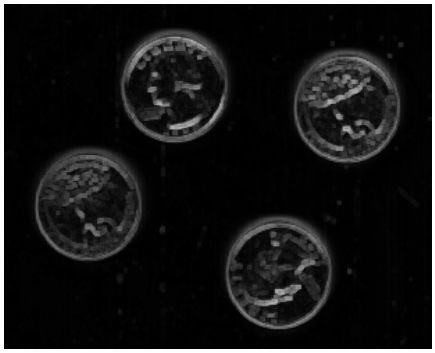

Figure 4.5: Range filtered image

4.9 TEXTURE SEGMENTATION EXAMPLE

As a basic test for the segmentation step of the algorithm, synthetic compositions of gray-scaled textures were. Unsupervised texture segmentation in a deterministic annealing framework.

Each of the compositions consists of five different textures. Segmentation algorithm is applied with windows of 32x32 pixels size, grid shift of 8 pixels, L=3 wavelet decomposition levels with rbio_3.3 and db4 wavelet filters. Both filters provided us with similar results shown below:

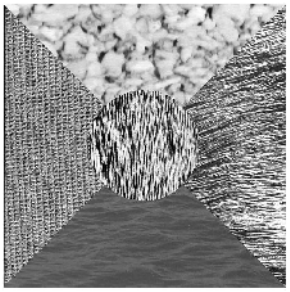

(a)

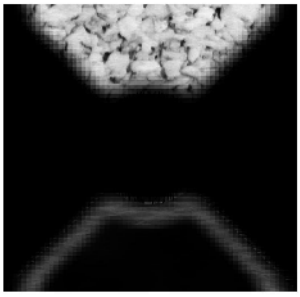

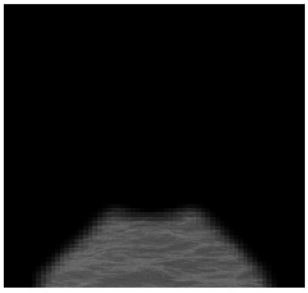

(b) (c)

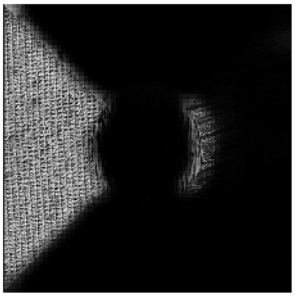

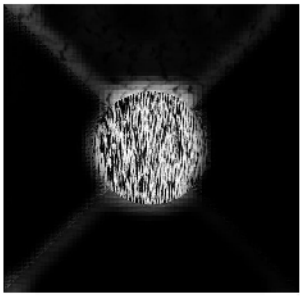

(d) (e)

Figure 4.6: Texture Segmentation Example. (a) Original image consisting of 5 regions, each of different texture. (b). (c), (d). (e) are the obtained segmentation of the original image into 5 segments.

4.10 USING A GRAY-LEVEL CO-OCCURRENCE MATRIX (GLCM)

A statistical method of examining texture that considers the spatial relationship of pixels is the gray-level co-occurrence matrix (GLCM), also known as the gray-level spatial dependence matrix. The GLCM functions characterize the texture of an image by calculating how often pairs of pixel with specific values and in a specified spatial

relationship occur in an image, creating a GLCM, and then extracting statistical measures from this matrix. The texture filter functions, described in Using Texture Filter Functions, cannot provide information about shape, i.e., the spatial relationships of pixels in an image.

4.11 CREATING A GRAY-LEVEL CO-OCCURRENCE MATRIX

To create a GLCM, use the gray comatrix function. The gray comatrix function creates a gray-level co-occurrence matrix (GLCM) by calculating how often a pixel with the intensity (gray-level) value *i* occurs in a specific spatial relationship to a pixel with the value *j*. By default, the spatial relationship is defined as the pixel of interest and the pixel to its immediate right (horizontally adjacent), but you can specify other spatial relationships between the two pixels. Each element (*i,j*) in the resultant glcm is simply the sum of the number of times that the pixel with value *i* occurred in the specified spatial relationship to a pixel with value *j* in the input image. The number of gray levels in the image determines the size of the GLCM. By default, gray comatrix uses scaling to reduce the number of intensity values in an image to eight, but you can use the Num Levels and the Gray Limits parameters to control this scaling of gray levels. See the gray comatrix reference page for more information.

The gray-level co-occurrence matrix can reveal certain properties about the spatial distribution of the gray levels in the texture image. For example, if most of the entries in the GLCM are concentrated along the diagonal, the texture is coarse with respect to the specified offset. You can also derive several statistical measures from the GLCM.

To illustrate, the following figure shows how graycomatrix calculates the first three values in a GLCM. In the output GLCM, element (1,1) contains the value 1 because there is only one instance in the input image where two horizontally adjacent pixels have the values 1 and 1, respectively. glcm(1,2) contains the value 2 because there are two instances where two horizontally adjacent pixels have the values 1 and 2. Element (1,3) in the GLCM has the value 0 because there are no instances of two horizontally adjacent pixels with the values 1 and 3.graycomatrix continues processing the input image, scanning the image for other pixel pairs (*i,j*) and recording the sums in the corresponding elements of the GLCM.

4.12 SPECIFYING THE OFFSETS

By default, the graycomatrix function creates a single GLCM, with the spatial relationship, or offset, defined as two horizontally adjacent pixels. However, a single GLCM might not be enough to describe the textural features of the input image. For example, a single horizontal offset might not be sensitive to texture with a vertical orientation. For this reason, graycomatrix can create multiple GLCMs for a single input image.

To create multiple GLCMs, specify an array of offsets to the graycomatrix function. These offsets define pixel relationships of varying direction and distance. For example, you can define an array of offsets that specify four directions (horizontal, vertical, and two diagonals) and four distances. In this case, the input image is represented by 16 GLCMs.

These offsets are specified as a *p*-by-2 array of integers. Each row in the array is a two-element vector,[row_offset, col_offset], that specifies one offset. row_offset is the number of rows between the pixel of interest and its neighbour col_offset is the number of columns between the pixel of interest and its neighbor. This example creates an offset that specifies four directions and 4 distances for each direction.

```
offsets = [ 0 1; 0 2; 0 3; 0 4;...
        -1 1; -2 2; -3 3; -4 4;...
        -1 0; -2 0; -3 0; -4 0;...
        -1 -1; -2 -2; -3 -3; -4 -4];
```

The figure illustrates the spatial relationships of pixels that are defined by this array of offsets, where D represents the distance from the pixel of interest.

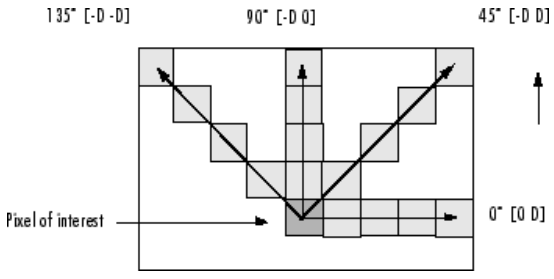

Figure 4.7: Specification of offset

4.13 CONTENT COMPARISON TECHNIQUES

The sections below describe common methods for extracting content from images so that they can be easily compared. The methods outlined are not specific to any particular application domain.

4.13.1 COLOR

Retrieving images based on color similarity is achieved by computing a color histogram for each image that identifies the proportion of pixels within an image holding specific values (that humans express as colors). Current research is attempting to segment color proportion by region and by spatial relationship among several color regions. Examining images based on the colors they contain is one of the most widely used techniques because it does not depend on image size or orientation. Color searches will usually involve comparing color histograms, though this is not the only technique in practice.

4.13.2 TEXTURE

Texture measures look for visual patterns in images and how they are spatially defined. Textures are represented by texels which are then placed into a number of sets, depending on how many textures are detected in the image. These sets not only define the texture, but also where in the image the texture is located. Texture is a difficult concept to represent. The identification of specific textures in an image is achieved primarily by modeling texture as a two-dimensional gray level variation. The relative brightness of pairs of pixels is computed such that degree of contrast, regularity, coarseness and directionality may be estimated. However, the problem is in identifying patterns of co-pixel variation and associating them with particular classes of textures such as silky, or rough.

4.13.3 SHAPE

Shape does not refer to the shape of an image but to the shape of a particular region that is being sought out. Shapes will often be determined first applying segmentation or edge detection to an image. Other methods use shape filters to identify given shapes of an image. In some cases accurate shape detection will require human intervention because methods like segmentation are very difficult to completely automate.

4.14 DERIVING STATISTICS FROM A GLCM

After GLCMs is created, several statistics are derived from them using the graycoprops function. These statistics provide information about the texture of an image.

Table 4.1: Texture features

Statistic	**Description**
CONTRAST	Measures the local variations in the gray-level co-occurrence matrix.
CORRELATION	Measures the joint probability occurrence of the specified pixel pairs.
ENERGY	Provides the sum of squared elements in the GLCM. Also known as uniformity or the angular second moment.
HOMOGENEITY	Measures the closeness of the distribution of elements in the GLCM to the GLCM diagonal.

The texture features that are considered in the system include:

1. Fractal dimension,
2. Coarseness,
3. Entropy,
4. Contrast
5. Correlation
6. Energy
7. Homogeneity

The reason for choosing these features is to facilitate the extraction of the most prominent texture features at various resolution, which is essential in the progressive feature extraction algorithm.

4.14.1 FRACTAL DIMENSION

Fractal dimension of a random function $I(x)$ is defined as $T+1-H$ where T is the topological dimension of $I(x)$, while H is a parameter of the fractal Brownian function $I(x)$ if for all x and Δx:

$$\Pr\left(\frac{(\quad+\Delta x)-I(x)}{\|\Delta x\|}\right)<y = F(y) \qquad 4.9$$

Fractal dimension one means of measuring disordered texture. In particular, it is useful to measure the surface roughness. It is chosen in our system because of its invariance to linear transformation of the data and the transformation of the scale. For our system, the reticular cell counting method, in which the number of cubes at different scales that are passed by the image surface are counted, is used to compute the fractal dimension.

4.14.2 COARSENESS

It is defined as

$$C = 1 - \frac{\qquad}{\qquad} \qquad 4.10$$

It is related to the dispersion of the image, S_D, defined as

$$S_D = \sum \qquad (i - S\ )\ h[i] \qquad 4.11$$

where S_M is the mean of the histogram,

h[i], of the image, and

L is the number of levels used in accumulating the histogram.

4.14.3 ENTROPY

It is defined as

$$\sum \sum \quad [\ ,\ \lg\ \ [\ ,\ ] \qquad 4.12$$

Measures the randomness of a gray-level distribution. The Entropy is expected to be high if the gray levels are distributed randomly throughout the image.

4.14.4 CONTRAST

The contrast ratio is a measure of a display system, defined as the ratio of the luminance of the brightest color (white) to that of the darkest color (black) that the system is capable of producing. A high contrast ratio is a desired aspect of any display, but with the various methods of measurement for a system or its part, remarkably different measured values can sometimes produce similar results.

$$\sum_{,} |\quad - \quad|_{p(i,j)} \qquad 4.13$$

Measures the local contrast of an image. The Contrast is expected to be low if the gray levels of each pixel pair are similar.

4.14.5 CORRELATION

It provides a correlation between the two pixels in the pixel pair. The Correlation is expected to be high if the gray levels of the pixel pairs are highly correlated.

$$\sum_{,} \frac{(\quad)(\quad)(\quad(\ ,\ )}{} \qquad 4.14$$

The correlation operation is defined mathematically as:

$$h(x) = f(x).g(x) = \int \quad ^{*}(\tau)g(x+\tau)d\tau \qquad 4.15$$

The f* (τ) is the complex conjugate of f (τ), but since this section will discuss correlation for signals which only contain real values, substitute f(τ).

Correlation is useful for feature detection; applying correlation to an image that possibly contains a target feature and an image of that feature forms local maxima or pixel value spikes in candidate positions.

This is useful in detecting letters on a page, or the position of armaments on a battlefield. Correlation can also be used to detect motion, such as the velocity of hurricanes in a satellite image or the jittering of an unsteady camera.

4.14.6 ENERGY

It Measures the number of repeated pairs. The Energy is expected to be high if the occurrence of repeated pixel pairs is high.

$$\sum_{,} \quad (\ ,\ ) \qquad 4.16$$

The histogram of smoothed texture energy image is shown below:

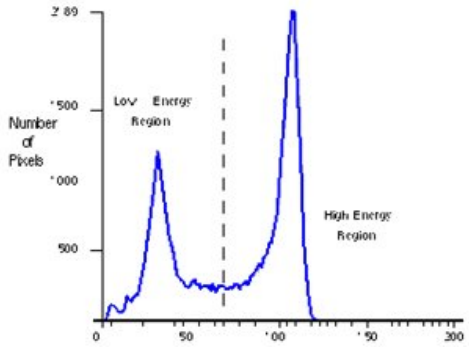

Figure 4.8: Histogram of texture energy image used in threshold segmentation

4.14.7 HOMOGENEITY

It means having the property that if each variable is replaced by a constant times that variable the constant can be factored out, having each term of the same degree if all variables are considered as homogeneous.

$$\sum , \frac{(,)}{|} | \qquad 4.17$$

4.15 APPLICATIONS OF TEXTURE SEGMENTATION:

Some software producers are trying to push Content Based Image Retrieval based applications into the filtering and law enforcement markets for the purpose of identifying and censoring images with skin-tones and shapes that could indicate controversial results.

4.16 CONCLUSION

Texture analysis is the method of algorithmically constructing a large digital image from a small digital sample image by taking advantage of its structural content. It includes contrast, correlation, homogeneity, energy and entropy of an image. This analysis can be used in many digital images also in the development of the films.

CHAPTER 5
METHODOLOGY

5.1 INTRODUCTION

For analyzing the textures, digital images are used and digital image processing is the use of computer algorithms to perform image processing on digital images. As a subfield of digital signal processing, digital image processing has many advantages over analog image processing; it allows a much wider range of algorithms to be applied to the input data, and can avoid problems such as the build-up of noise and signal distortion during processing. The digital image processing is done by special software programs that can manipulate the images in many ways.

It allows the use of much more complex algorithms for image processing, and hence can offer both more sophisticated performance at simple tasks, and the implementation of methods which would be impossible by analog means.

5.2 DIGITAL CAMERA IMAGES

Digital cameras generally include dedicated digital image processing chips to convert the raw data from the image sensor into a color-corrected image in a standard image file format. Images from digital cameras often receive further processing to improve their quality, distinct advantage digital cameras have over film cameras. The digital image processing is typically done by special software programs that can manipulate the images in many ways.

5.3 MATLAB SOFTWARE

This high-performance language for technical computing integrates computation, visualization, and programming in an easy-to-use environment where problems and solutions are expressed in familiar mathematical notation.

Typical uses include:

1. Math and computation
2. Algorithm development
3. Data acquisition
4. Modeling, simulation, and prototyping
5. Data analysis, exploration, and visualization
6. Scientific and engineering graphics
7. Application development, including graphical user interface building

MATLAB is an interactive system whose basic data element is an array that does not require dimensioning. It allows you to solve many technical computing problems, especially those with matrix and vector formulations, in a fraction of the time it would take to write a program in a scalar non interactive language such as C or Fortran.

The name Matlab stands for matrix laboratory. It was originally written to provide easy access to matrix software developed by the LINPACK and EISPACK projects. Today, MATLAB engines incorporate the LAPACK and BLAS libraries, embedding the state of the art in software for matrix computation.

Matlab has evolved over a period of years with input from many users. In university environments, it is the standard instructional tool for introductory and advanced courses in mathematics, engineering, and science. In industry, matlab is the tool of choice for high-productivity research, development, and analysis. It features a family of add-on application-specific solutions called toolboxes. Very important to most of its users, toolboxes allow learning and applying specialized technology. Toolboxes are comprehensive collections of Matlab functions (M-files) that extend its environment to solve particular classes of problems.

5.4 FLOWCHART FOR THE DETERMINATION OF THE ABNORMLITIES IN BIOMEDICAL IMGAE USING TEXTURE SEGMENTATION

The detection of defects in biomedical images using texture texture segmentation is shown in the flowchart given below:

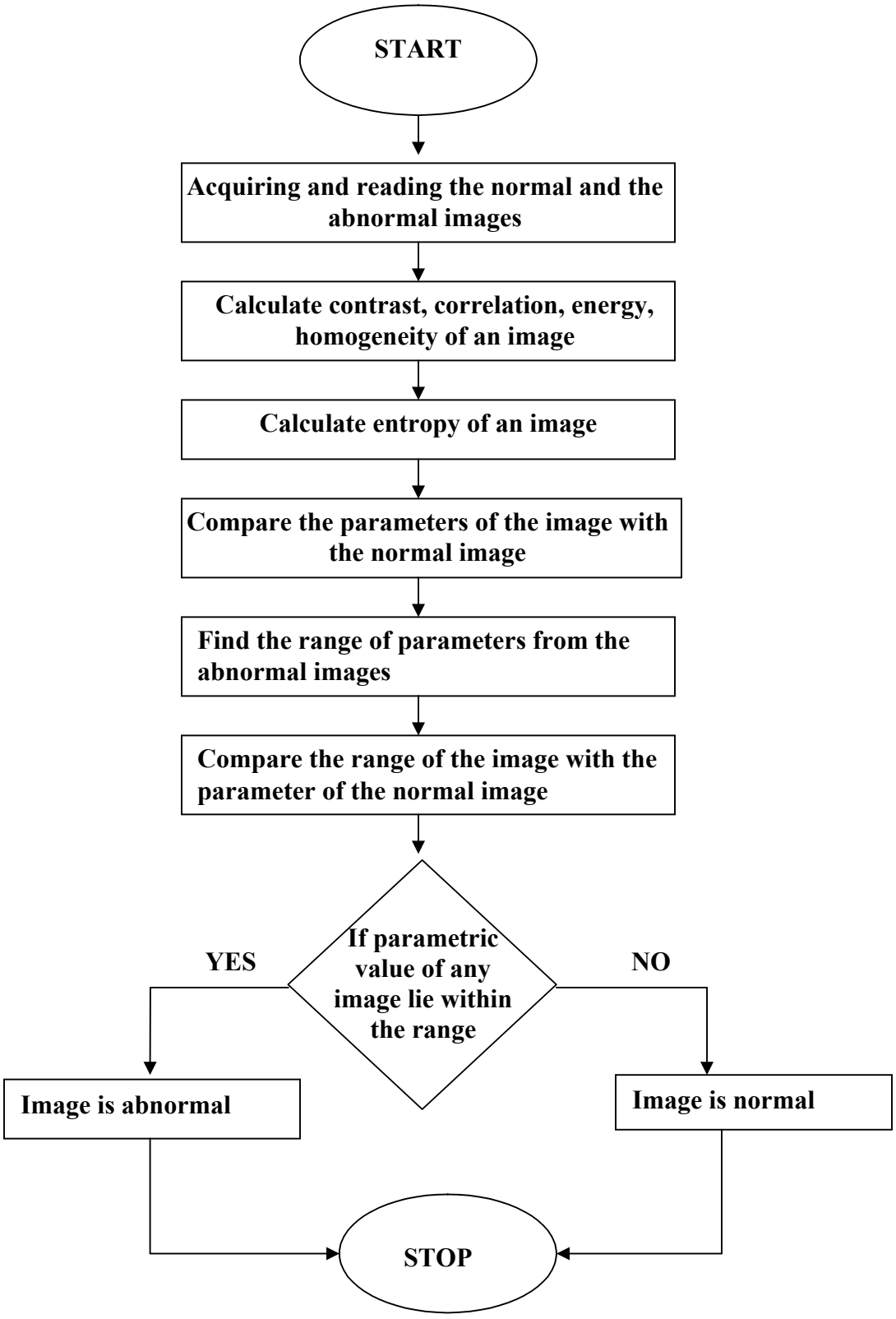

Figure 5.1: Flowchart for the determination of normal and abnormality image

5.5 ALGORITHM FOR THE DETERMINATION OF THE ABNORMLITIES IN BIOMEDICAL IMAGE USING TEXTURE SEGMENTATION

The detection of defects in biomedical images using texture texture segmentation is shown in the algorithm given below:

STEP 1: Firstly the normal and abnormal images are read by using imread command. This is an inbuilt command of matlab for reading the image, image is read when the image name along with its extension is given otherwise error will be generated.

$$A = \text{imread(filename,fmt)} \tag{5.1}$$

It reads a grayscale or color image from the file specified by the string filename, where the string fmt specifies the format of the file. If the file is not in the current directory or in a directory in the Matlab path, specify the full pathname of the location on your system. imread returns the image data in the array A. If the file contains a grayscale image, A is a two-dimensional(M-by-N) array. If the file contains a color image, A is a three-dimensional (M-by-N-by-3) array. The class of the returned array depends on the data type used by the file format. For TIFF files, however, imread can return color data that uses the RGB, CIELAB, ICCLAB, or CMYK color spaces. If the color image uses the CMYK color space, A is an M-by-N-by-4 array.

STEP 2: Calculate the contrast, correlation, homogeneity and energy of the abnormal images. These parameters can be calculated by using graycoprops command, which also being a inbuilt function.

$$\text{stats} = \text{graycoprops(glcm, properties)} \tag{5.2}$$

It calculates the statistics specified in properties from the gray-level co-occurence matrix glcm. glcm is an m-by-n-by-p array of valid gray-level co-occurrence matrices. If glcm is an array of GLCMs, stats is an array of statistics for each glcm.graycoprops normalizes the gray-level co-occurrence matrix (GLCM) so that the sum of its elements is equal to 1.

Each element (r,c) in the normalized GLCM is the joint probability occurrence of pixel pairs with a defined spatial relationship having gray level values r and c in the image. graycoprops uses the normalized GLCM to calculate properties.

Table 5.1: Properties of Texture

Property	Description	Formula
Contrast	Returns a measure of the intensity contrast between a pixel and its neighbor over the whole image. Range = [0 (size(GLCM,1)-1)^2] Contrast is 0 for a constant image	$\sum_{,} \lvert \quad - \quad \rvert_{p(i,j)}$
Correlation	Returns a measure of how correlated a pixel is to its neighbor over the whole image. Range = [-1 1] Correlation is 1 or -1 for a perfectly positively or negatively correlated image. Correlation is NaN for a constant image.	$\frac{(\quad -\mu)(\quad -\mu\ )(\quad (\ ,\ )}{,}$
Energy	Returns the sum of squared elements in the GLCM .Range = [0 1] Energy is 1 for a constant image.	$(\ ,\ )$,
Homogeneity	Returns a value that measures the closeness of the distribution of elements in the GLCM to the GLCM diagonal. Range = [0 1] Homogeneity is 1 for a diagonal GLCM.	$\frac{(\ ,\ )}{1+\lvert \quad - \quad \rvert}$,

STEP 3: Calculate the entropy of the abnormal images using entropy function of matlab.

$$E = \text{entropy}(I) \quad 5.3$$

It measures the randomness of a gray-level distribution. The Entropy is expected to be high if the gray levels are distributed randomly throughout the image.

$$-\sum \sum [\ ,\ \text{lg}\ [\ ,\ ] \quad 5.4$$

It returns E, a scalar value representing the entropy of grayscale image I. Entropy is a statistical measure of randomness that can be used to characterize the texture of the input image. Entropy is defined as -sum (p.*log (p)) where p contains the histogram counts returned from imhist. By default, entropy uses two bins for logical arrays and 256 bins for uint8, uint16, or double arrays. I can be a multidimensional image. If I has more than two dimensions, the entropy function treats it as a multidimensional grayscale image and not as an RGB image.

STEP 4: Now, find the parameters of the normal image using graycoprops and entropy function are the inbuilt functions of the matlab.

STEP 5: Find the range of the parameters of the abnormal images.

STEP 6: Compare the parameter of the normal image and the parameters of the abnormal images. It will be observed that the normal image parameters do not lie within the range.

STEP 7: Finally, a conclusion is obtained that the image parameters lying within the range is the abnormal image and consists of tumor. Hence, the report of the patient is positive and consists of abnormality.

5.6 CONCLUSION

In this chapter the MR images are taken and after applying texture segmentation in these images using matlab software, the textures of both normal and abnormal images are obtained. On the bases of comparison between the ranges of abnormal MR image normal image, the defected image is finally detected.

CHAPTER 6
RESULTS AND DISCUSSIONS

6.1 INTRODUCTION

In this, the detection of abnormality in the patient's image is automatically recognized using texture analysis. This chapter include following steps to finally conclude the abnormality:

1. Texture Features Analysis of abnormal and normal images.
2. Tabular formulation of the texture features of normal and abnormal images.
3. Determination of range of all contrast of all cases.
4. Determination of range of all correlation of all cases.
5. Determination of range of all energy of all cases.
6. Determination of range of all homogeneity of all cases.
7. Determination of range of all entropy of all cases.
8. Graphical representation of the parameters of the normal and abnormal images for all the 5 cases

6.2 TEXTURE FEATURES ANALYSIS OF ABNORMAL AND NORMAL IMAGES

In this, 5 different abnormal MR images of different parts brain and different textures features are calculated as shown in Table 5.1. For that particular part, a normal image is taken. The texture analysis of the normal image is also done.

Table 6.1: Texture features analysis of different MR image

Case	Image Type	Image No.		Texture Features
I	**Normal**	**I**		**Contrast: 2.2723** **Correlation: -0.0042** **Energy: 1.5590** **Homogeneity:0.0249** **Entropy : 6.6597**
	Abnormal	II	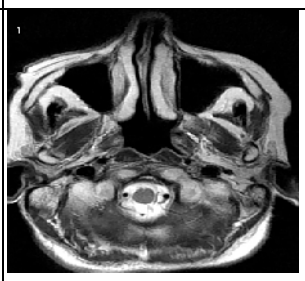	Contrast: 2.0134 Correlation: -0.0034 Energy: 1.5784 Homogeneity: 0.0277 Entropy : 6.9580
	Abnormal	III	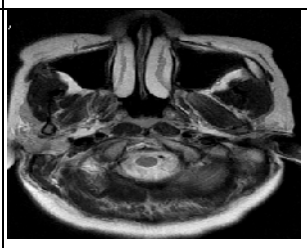	Contrast: 2.1638 Correlation:-0.0035 Energy:1.6239 Homogeneity:0.0268 Entropy:6.8663
	Abnormal	IV		Contrast:2.0840 Correlation: -0.0029 Energy: 1.6241 Homogeneity: 0.0271 Entropy :6.7876
	Abnormal	V		Contrast:1.8478 Correlation: -8.0489 Energy: 1.6949 Homogeneity:0.0284 Entropy :6.7175

	Abnormal	VI	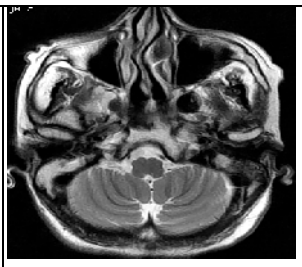	Contrast:1.8928 Correlation: 1.9322 Energy:1.5644 Homogeneity: 0.0287 Entropy :7.0244
II	**Normal**	**VII**	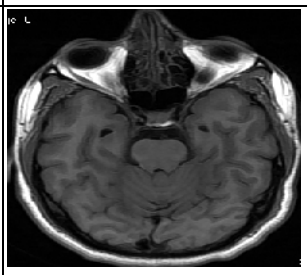	**Contrast: 2.5099** **Correlation: -0.0051** **Energy:1.4734** **Homogeneity: 0.0249** **Entropy:6.5689**
	Abnormal	VIII	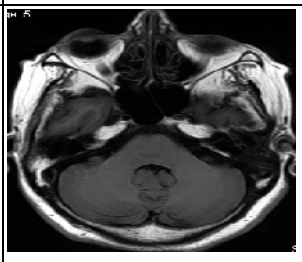	Contrast:2.4141 Correlation:0.0025 Energy:1.7360 Homogeneity: 0.0259 Entropy :6.9954
	Abnormal	IX	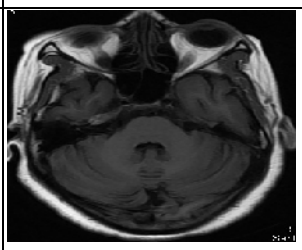	Contrast:2.4732 Correlation: [0.0036 Energy:1.6021 Homogeneity:0.0252 Entropy :6.7010
	Abnormal	X	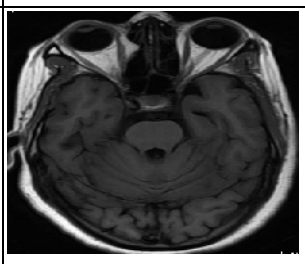	Contrast:2.3772 Correlation:0.0063 Energy:1.5917e-005 Homogeneity:0.0261 Entropy :6.7137

	Abnormal	XI	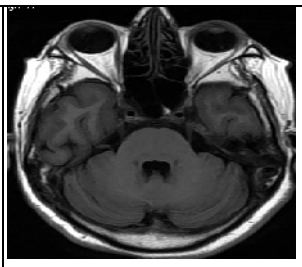	Contrast:2.4002 Correlation:0.0018 Energy:1.6940 Homogeneity:0.0256 Entropy:6.9779
	Abnormal	XII	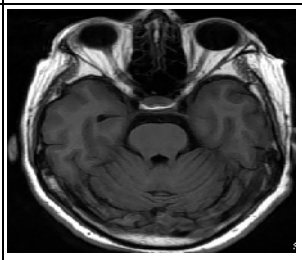	Contrast: 2.2711 Correlation:-0.0042 Energy:1.5752e-005 Homogeneity:0.0261 Entropy:6.9708
III	**Normal**	**XIII**	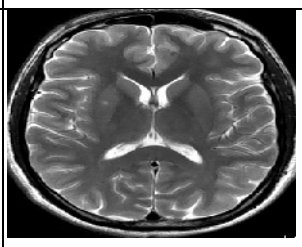	**Contrast: 2.9791** **Correlation: -0.0052** **Energy: 1.2990** **Homogeneity: 0.0245** **Entropy :6.8942**
	Abnormal	XIV		Contrast:2.0204 Correlation:-0.0085 Energy:1.3585 Homogeneity:0.0280 Entropy :7.1366
	Abnormal	XV	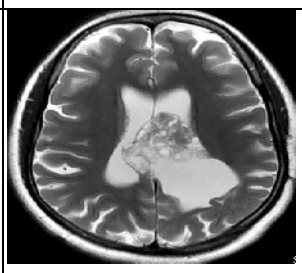	Contrast:1.9172 Correlation:-0.0048 Energy:1.3793e-005 Homogeneity: 0.0283 Entropy :7.1363

	Abnormal	XVI	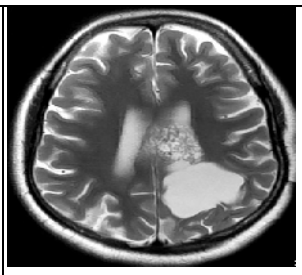	Contrast: 1.9542 Correlation:-0.0019 Energy:1.3716 Homogeneity: 0.0281 Entropy:7.0017
	Abnormal	XVII	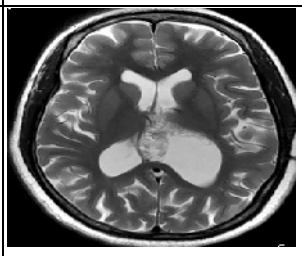	Contrast:2.0447 Correlation: -0.0038 Energy:1.3464 Homogeneity:0.0273 Entropy:=7.1204
	Abnormal	XVIII	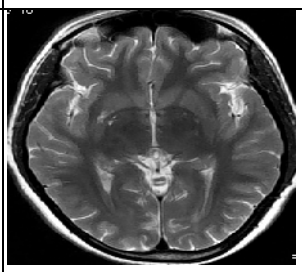	Contrast:2.0927 Correlation: 0.0251 Energy: 1.3542e-005 Homogeneity: 0.0254 Entropy:6.9111
IV	**Normal**	**XIX**	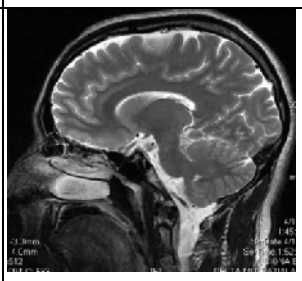	**Contrast:2.6184** **Correlation:0.0196** **Energy:7.2459e-006** **Homogeneity:0.0243** **Entropy :7.0265**
	Abnormal	XX	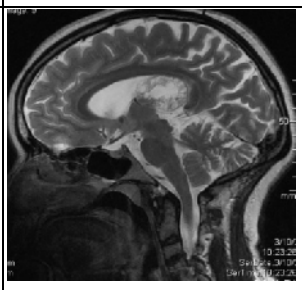	Contrast:2.7552 Correlation:-0.0141 Energy:9.2043 Homogeneity:0.0252 Entropy :7.1720

	Abnormal	XXI		Contrast:2.7759 Correlation: 0.0027 Energy:7.8468 Homogeneity:0.0249 Entropy :7.5112
	Abnormal	XXII		Contrast:2.7493 Correlation: -0.0153 Energy: 9.6926 Homogeneity:0.0251 Entropy :7.5064
	Abnormal	XXIII		Contrast:2.7174 Correlation:0.0062 Energy:9.8728 Homogeneity:0.0249 Entropy :7.3821
	Abnormal	XXIV		Contrast:2.6470 Correlation: 6.4667 Energy:7.9929 Homogeneity: 0.0245 Entropy:7.6010
V	**Normal**	**XXV**	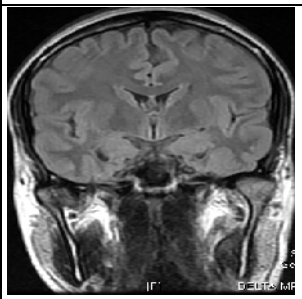	**Contrast: 2.8536** **Correlation:-0.0075** **Energy:1.1271** **Homogeneity:0.0233** **Entropy:7.4908**

	Abnormal	XXVI	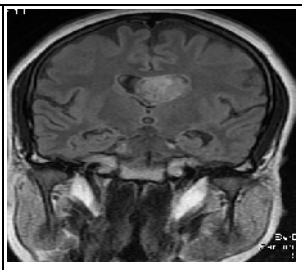	Contrast:2.7552 Correlation:0.0030 Energy:9.7187e-006 Homogeneity:0.0246 Entropy :7.3134
	Abnormal	XXVII	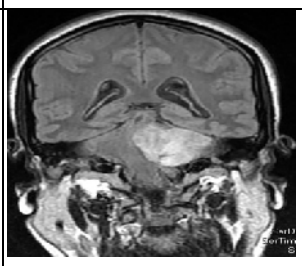	Contrast:2.2945 Correlation:-2.9908 Energy:1.0398 Homogeneity:0.0261 Entropy :7.5848
	Abnormal	XXVIII	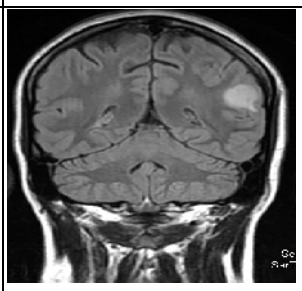	Contrast:2.0316 Correlation: -0.0029 Energy:1.2257 Homogeneity:0.0265 Entropy :7.2861
	Abnormal	XXIX	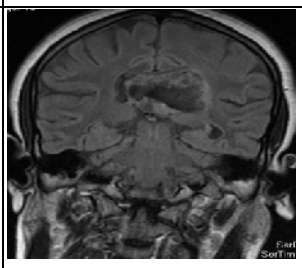	Contrast:2.4515 Correlation:-0.0058 Energy:9.9667e- Homogeneity:0.0254 Entropy:7.0256
	Abnormal	XXX	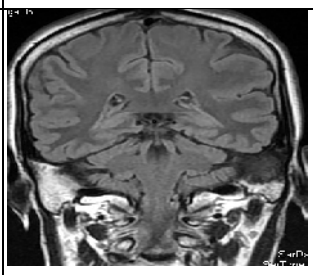	Contrast:2.6852 Correlation: 0.0691 Energy:8.5744 Homogeneity: 0.0246 Entropy::6.6039

6.3 TABULAR FORMATION OF THE TEXTURES FEATURES OF NORMAL AND ABNORMAL IMAGES

When all the textures analysis of the images is completed then the calculation of its range would be clearer by viewing it in tabular form.

Table 6.2: Texture features of different cases of abnormal and normal image

Case	Image Type	Image No.	Contrast	Correlation	Energy	Homog-eneity	Entropy
I	**Normal**	**I**	**2.2723**	**0.052**	**1.559**	**0.0249**	**6.6597**
	Abnormal	II	2.1638	0.0034	1.5784	0.0277	6.958
	Abnormal	III	2.0134	0.0035	1.6239	0.0268	6.8663
	Abnormal	IV	2.084	0.0029	1.6241	0.0271	6.7876
	Abnormal	V	1.8478	0.0489	1.6949	0.0284	6.7175
	Abnormal	VI	1.8928	0.047	1.5644	0.0287	7.0244
II	**Normal**	**VII**	**2.5099**	**0.0071**	**1.4734**	**0.0249**	**6.5689**
	Abnormal	VIII	2.4141	0.0025	1.736	0.0259	6.9954
	Abnormal	IX	2.4732	0.0036	1.6021	0.0252	6.701
	Abnormal	X	2.3772	0.0063	1.5917	0.0261	6.7137
	Abnormal	XI	2.4002	0.0018	1.694	0.0256	6.9779
	Abnormal	XII	2.271	0.0042	1.5752	0.0261	6.9708
III	**Normal**	**XIII**	**2.9791**	**0.052**	**1.299**	**0.0245**	**6.8942**
	Abnormal	XIV	2.0204	0.0085	1.3585	0.028	7.1366
	Abnormal	XV	1.9172	0.0048	1.3793	0.0283	7.1363
	Abnormal	XVI	1.9542	0.0019	1.3716	0.0281	7.0017
	Abnormal	XVII	2.0447	0.0038	1.3464	0.0273	7.1204
	Abnormal	XVIII	2.0927	0.0251	1.3542	0.0254	6.9111
IV	**Normal**	**XIX**	**2.6184**	**0.0196**	**7.2459**	**0.0243**	**7.0265**
	Abnormal	XX	2.7552	0.0141	9.2043	0.0252	7.172
	Abnormal	XXI	2.7759	0.0027	7.8468	0.0249	7.5112
	Abnormal	XXII	2.7493	0.0153	9.6926	0.0251	7.5064
	Abnormal	XXIII	2.7174	0.0062	9.8728	0.0249	7.3821
	Abnormal	XXIV	2.6700	0.0064	7.9929	0.0245	7.601
V	**Normal**	**XXV**	**2.6536**	**0.025**	**1.127**	**0.0233**	**7.4908**
	Abnormal	XXVI	2.5361	0.003	1.231	0.0246	7.3134
	Abnormal	XXVII	2.2945	0.0029	1.2398	0.0261	7.3848
	Abnormal	XXVIII	2.0316	0.0029	1.2257	0.0265	7.2861
	Abnormal	XXIX	2.4515	0.0058	1.2667	0.0254	7.0256
	Abnormal	XXX	2.6852	0.0069	1.255	0.0246	6.6039

6.4 DETERMINATION OF THE RANGE OF CONTRAST FOR ALL THE CASES

The contrast range can be obtained finding the maxima and minima of the abnormal images of the particular part and then comparing it with the normal image of that part.

Table 6.3: Contrast values of different cases

Case	Mean	Max.	Min.	Normal
I	2.0003	2.1638	1.8478	2.2723
II	2.3817	2.4732	2.271	2.5099
III	2.0058	2.0927	1.9172	2.9791
IV	2.7289	2.7759	2.647	2.6184
V	2.4436	2.7552	2.0316	2.8536

6.5 DETERMINATION OF THE RANGE OF CORRELATION FOR ALL THE CASES

The correlation range can be obtained finding the maxima and minima of the abnormal images of the particular part and then comparing it with the normal image of that part.

Table 6.4: Correlation values of different cases

Case	Mean	Max.	Min.	Normal
I	0.0211	0.0029	0.0481	0.052
II	0.0036	0.0063	0.0042	0.0071
III	0.0088	0.0251	0.0048	0.052
IV	0.0089	0.0064	0.0153	0.0196
V	0.0167	0.0691	0.0068	0.025

6.6 DETERMINATION OF THE RANGE OF ENERGY FOR ALL THE CASES

The energy range can be obtained finding the maxima and minima of the abnormal images of the particular part and then comparing it with the normal image of that part.

Table 6.5: Energy values of different cases

Case	Mean	Max.	Min.	Normal
I	1.6114	1.6949	1.5784	1.559
II	1.6398	1.736	1.5752	1.4734
III	1.362	1.3793	1.3464	1.299
IV	8.92188	9.8728	7.8468	7.2459
V	1.2435	1.266	1.231	1.127

6.7 DETERMINATION OF THE RANGE OF HOMOGENEITY FOR ALL THE CASES

The homogeneity range can be obtained finding the maxima and minima of the abnormal images of the particular part and then comparing it with the normal image of that part.

Table 6.6: Homogeneity values of different cases

Case	Mean	Max.	Min.	Normal
I	0.0277	0.0287	0.0268	0.0249
II	0.0257	0.0261	0.0252	0.0249
III	0.0274	0.0283	0.0254	0.0245
IV	0.0249	0.0252	0.0245	0.0243
V	0.0254	0.0265	0.0246	0.0233

6.8 DETERMINATION OF THE RANGE OF ENTROPY FOR ALL THE CASES

The entropy range can be obtained finding the maxima and minima of the abnormal images of the particular part and then comparing it with the normal image of that part.

Table 6.7: Entropy values of different cases

Case	Mean	Max.	Min.	Normal
I	6.8707	6.958	6.7175	6.6597
II	6.8717	6.9954	6.701	6.5689
III	7.0612	7.1366	6.9111	6.8942
IV	7.43454	7.601	7.172	7.0265
V	7.12276	7.3848	6.6039	7.4908

6.8 GRAPHICAL REPRESENTATION OF THE PARAMETERS OF THE NORMAL AND ABNORMAL IMAGES FOR ALL THE 5 CASES

The representation of the parameters graphically indicates visually the ranges that were tabularly obtained and makes the study more clear. This way the difference between the normal and abnormal image is obtained and can indicate whether the patient's report is positive and contains tumor or any abnormality.

CASE I

1. **Contrast**

   The contrast of the normal image for Case I is having the maximum value i.e. 2.2732 and is not within the range of the abnormal images.

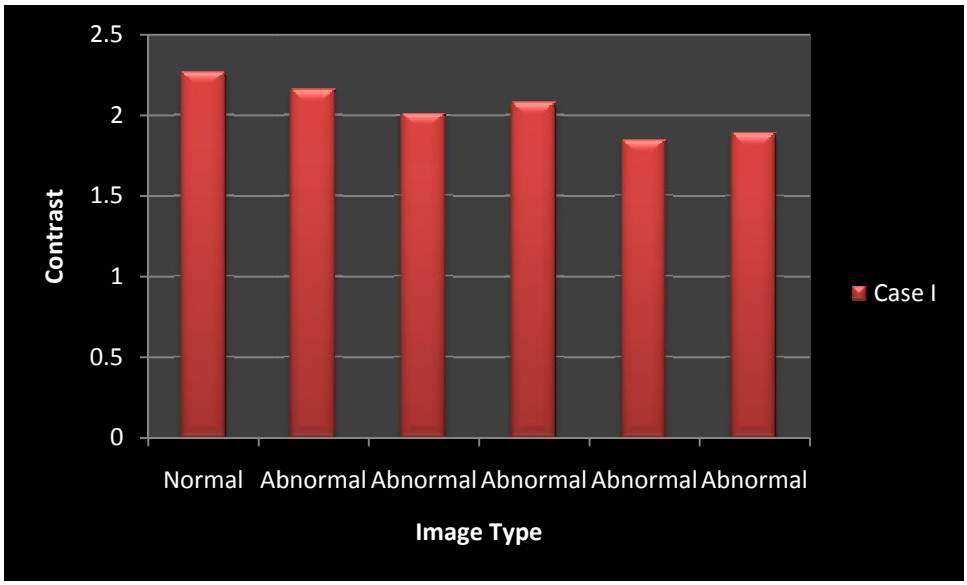

Figure 6.1 Comparison between the contrast of normal and abnormal image

2. CORRELATION

The correlation of the normal image for Case I is having the maximum value i.e. 0.0052 and is not within the range of the abnormal images.

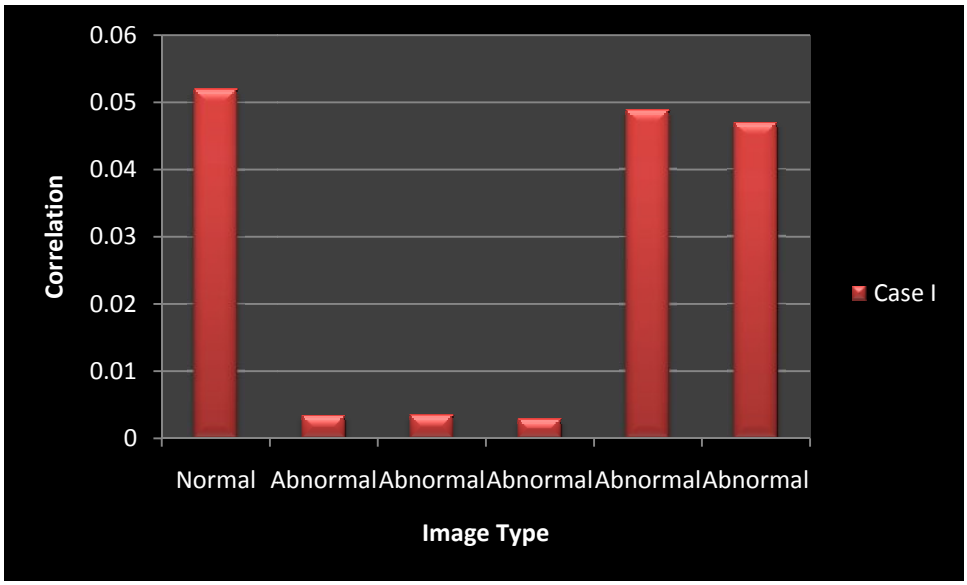

Figure 6.2 Comparison between the correlation of normal and abnormal image

3. ENERGY

The energy of the normal image for Case I is having the least value i.e. 1.559 and is not within the range of the abnormal images.

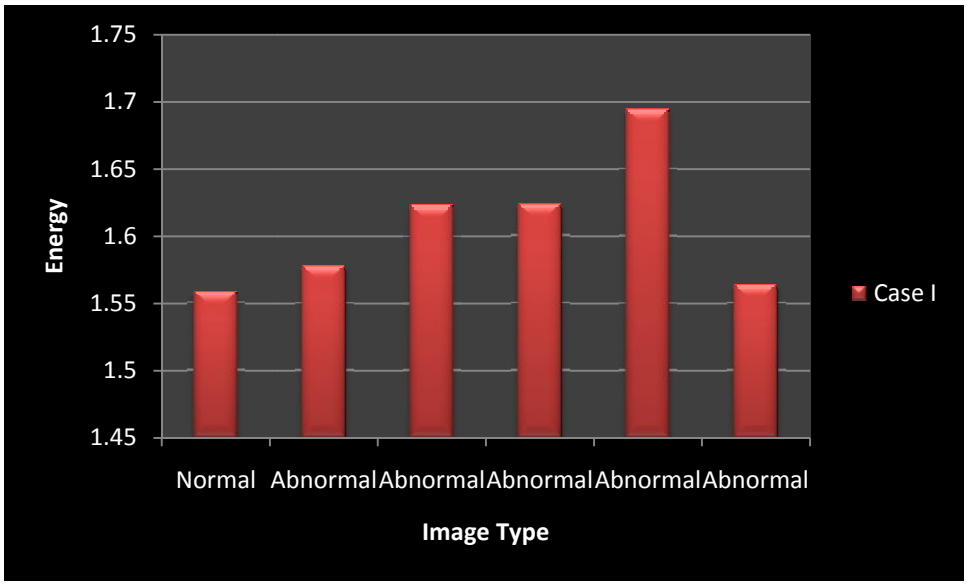

Figure 6.3 Comparison between the energy of normal and abnormal image

4. HOMOGENEITY

The homogeneity of the normal image for Case I is having the minimum value i.e. 0.0249 and is not within the range of the abnormal images.

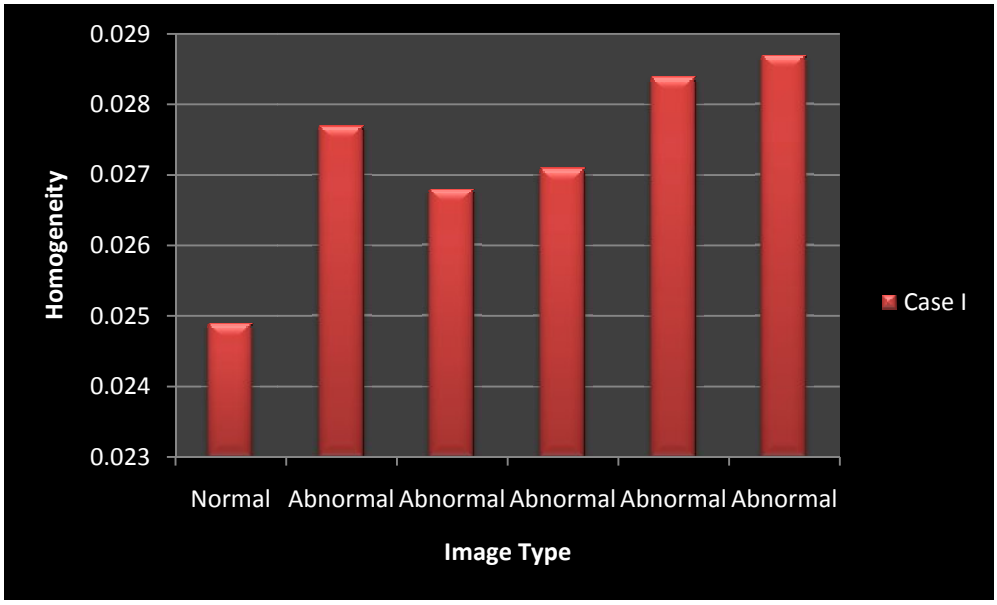

Figure 6.4 Comparison between the homogeneity of normal and abnormal image

5. ENTROPY

The entropy of the normal image for Case I is having the least value i.e. 6.6597 and is not within the range of the abnormal images.

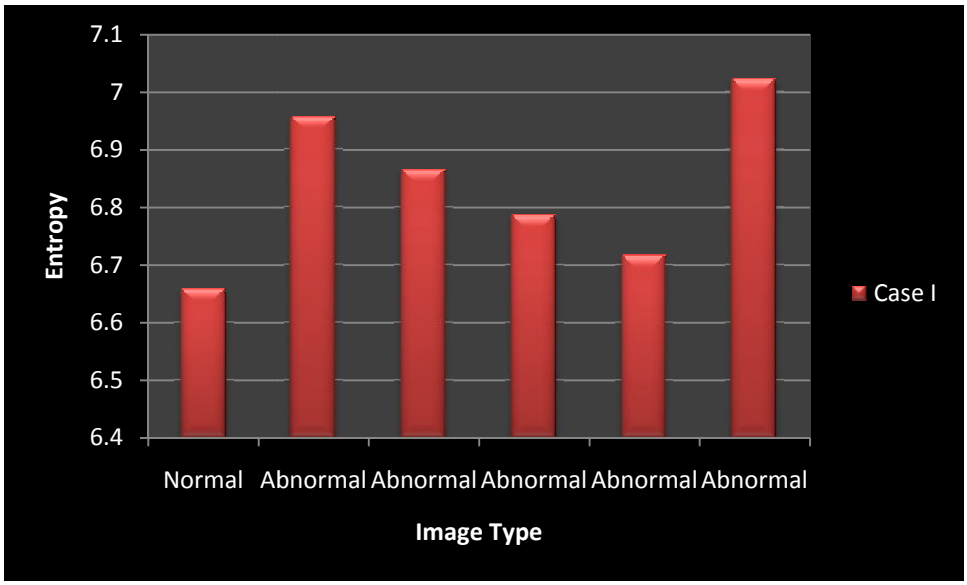

Figure 6.5 Comparison between the entropy of normal and abnormal image

CASE II

1. CONTRAST

The contrast of the normal image for Case II is having the maximum value i.e. 2.5099 and is not within the range of the abnormal images.

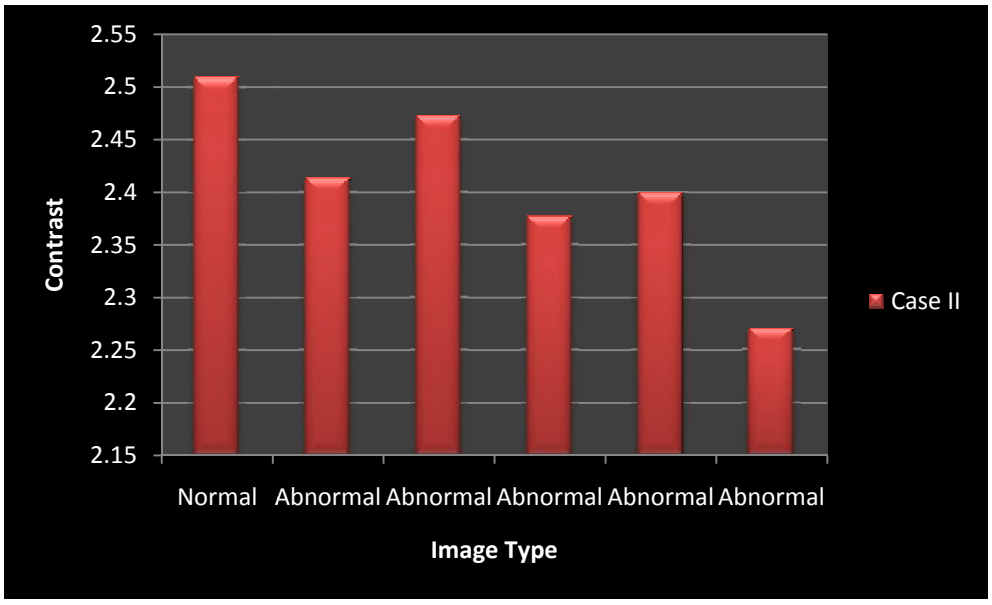

Figure 6.6 Comparison between the contrast of normal and abnormal image

2. CORRELATION

The correlation of the normal image for Case II is having the maximum value i.e. 0.0071 and is not within the range of the abnormal images.

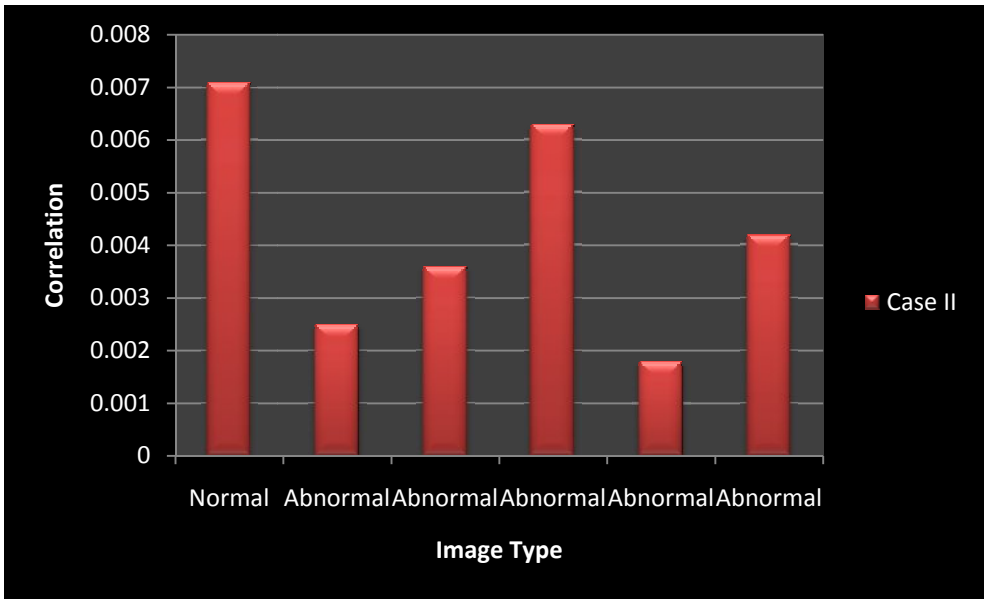

Figure 6.7 Comparison between the contrast of correlation and abnormal image

3. ENERGY

The energy of the normal image for Case II is having the least value i.e. 1.4734 and is not within the range of the abnormal images.

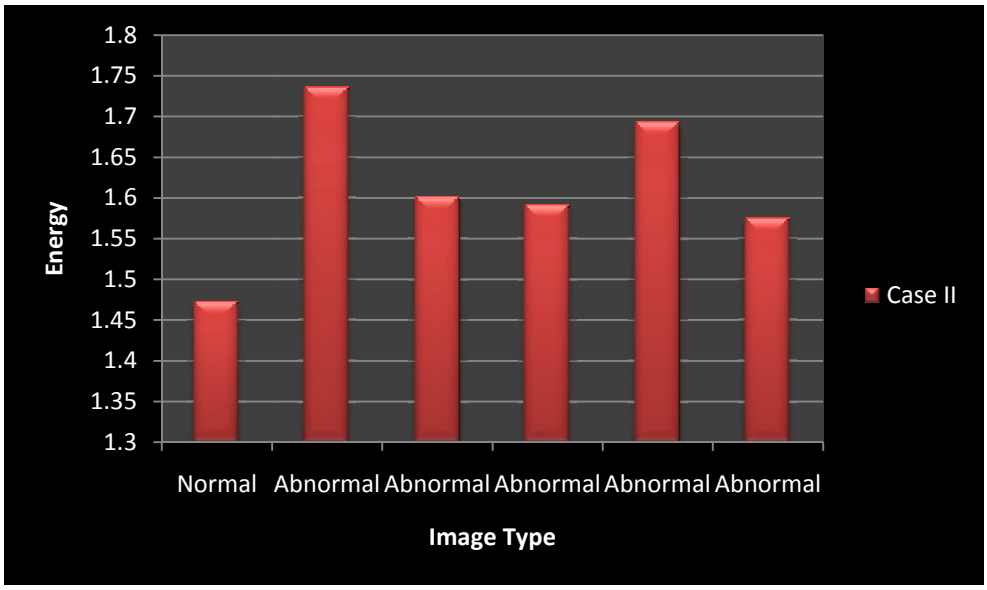

Figure 6.8 Comparison between the energy of normal and abnormal image

4. HOMOGENEITY

The homogeneity of the normal image for Case II is having the mimimum value i.e. 0.0249 and is not within the range of the abnormal images.

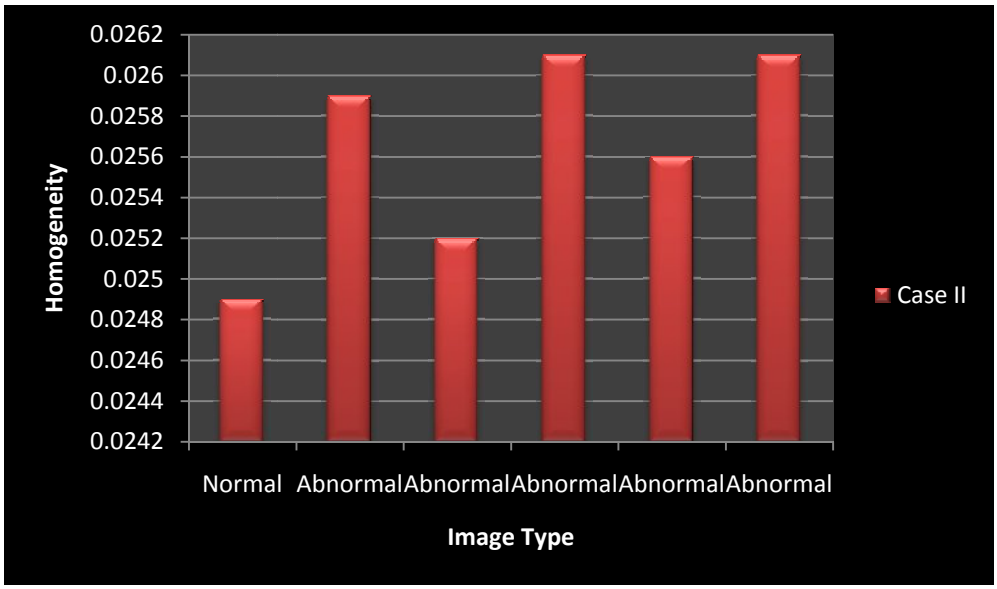

Figure 6.9 Comparison between the homogeneity of normal and abnormal image

5. ENTROPY

The entropy of the normal image for Case II is having the least value i.e. 6.5689 and is not within the range of the abnormal images.

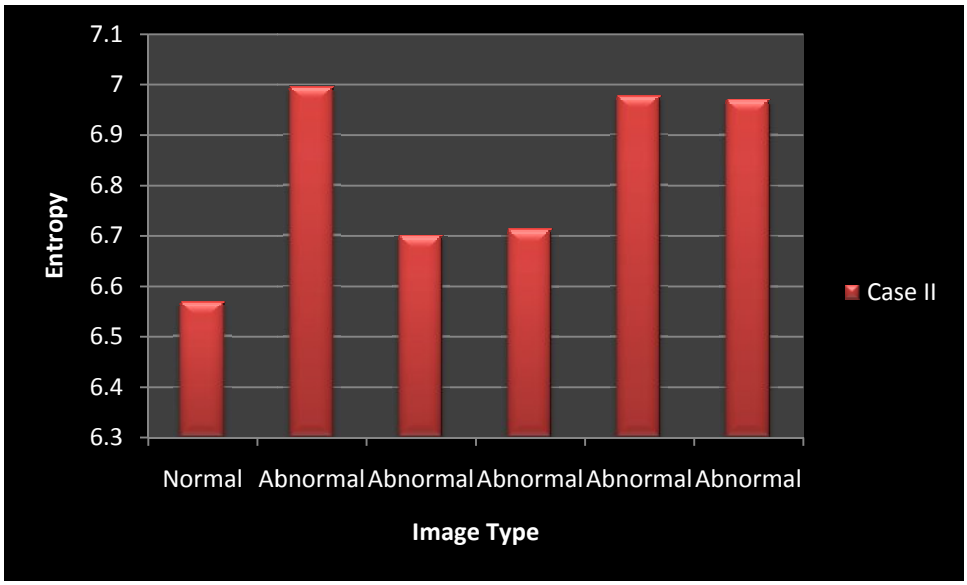

Figure 6.10 Comparison between the entropy of normal and abnormal image

CASE III

1. CONTRAST

The contrast of the normal image for Case III is having the maximum value i.e. 2.0791 and is not within the range of the abnormal images.

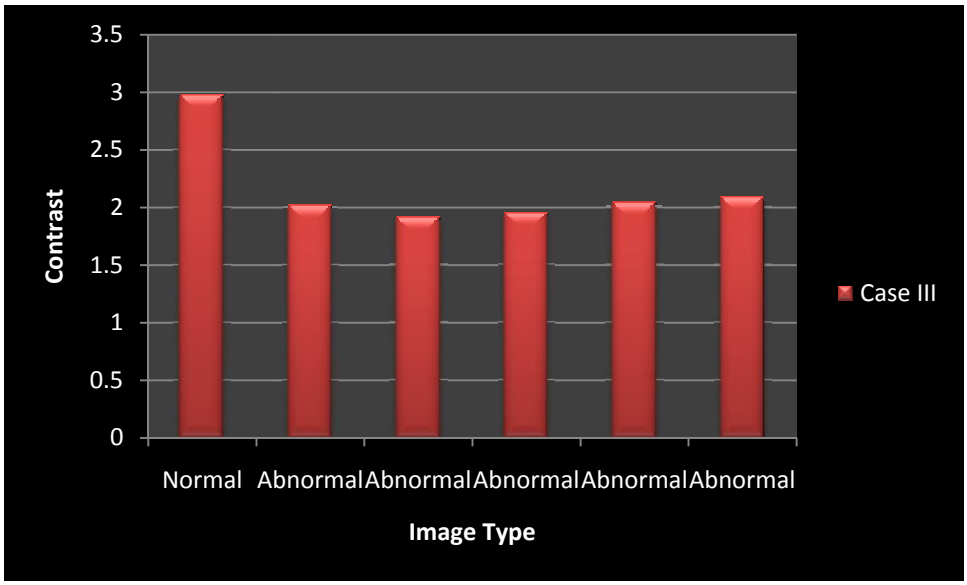

Figure 6.11 Comparison between the contrast of normal and abnormal image

2. CORRELATION

The correlation of the normal image for Case III is having the maximum value i.e. 0.052 and is not within the range of the abnormal images.

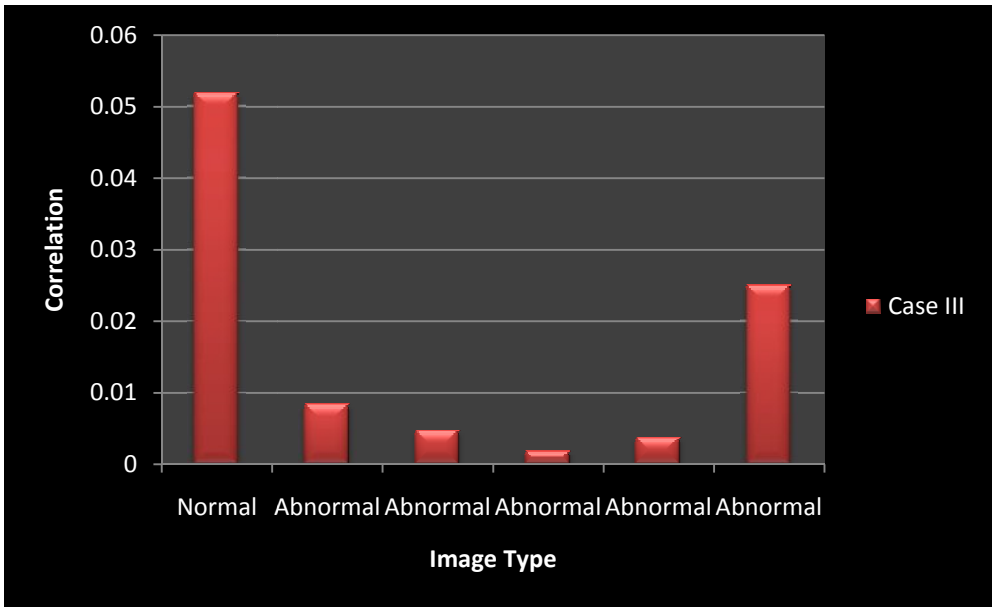

Figure 6.12 Comparison between the correlation of normal and abnormal image

3. ENERGY

The energy of the normal image for Case III is having the least value i.e. 1.299 and is not within the range of the abnormal images.

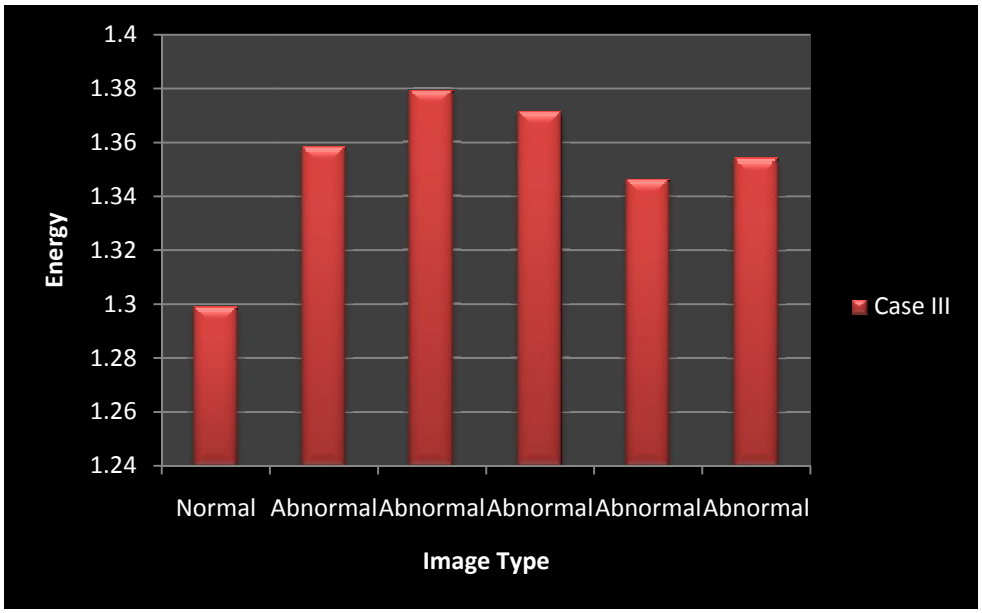

Figure 6.13 Comparison between the correlation of normal and abnormal image

4. HOMOGENEITY

The homogeneity of the normal image for Case III is having the least value i.e. 0.0245 and is not within the range of the abnormal images.

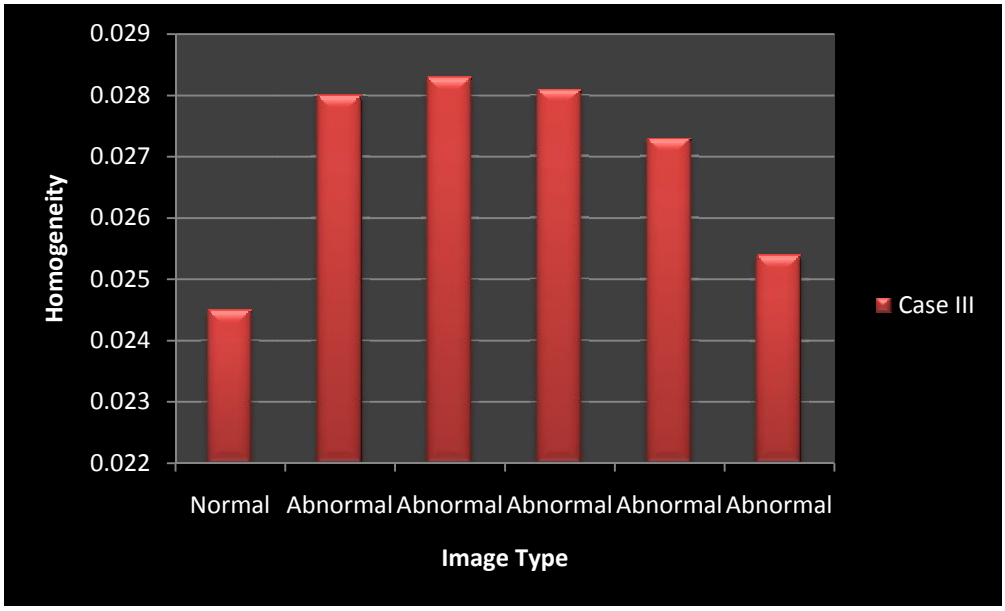

Figure 6.14 Comparison between the homogeneity of normal and abnormal image

5. ENTROPY

The entropy of the normal image for Case III is having the least value i.e. 6.8942 and is not within the range of the abnormal images.

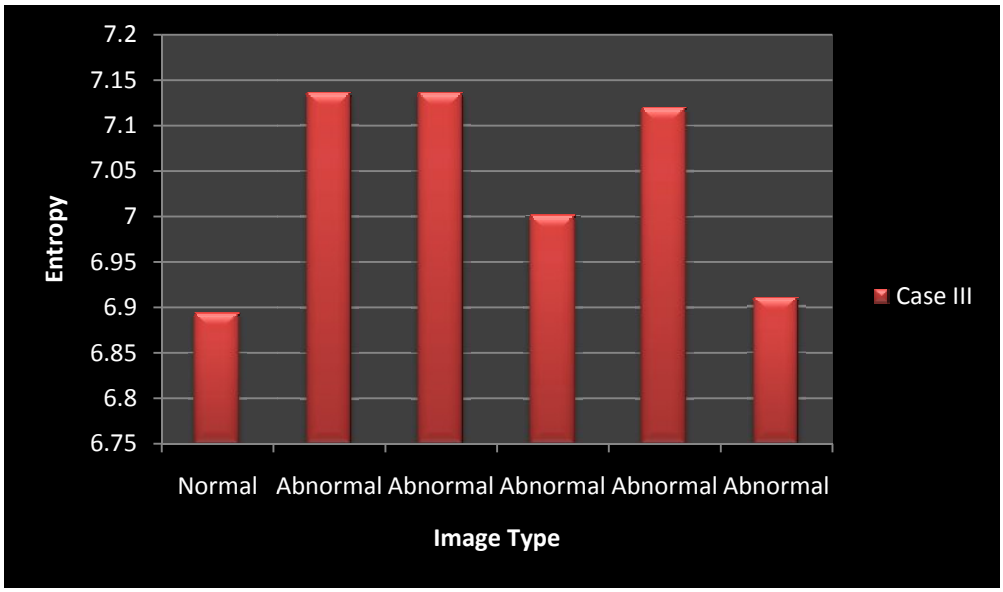

Figure 6.15 Comparison between the entropy of normal and abnormal image

CASE IV

1. CONTRAST

The contrast of the normal image for Case IV is having the least value i.e. 2.6184 and is not within the range of the abnormal images.

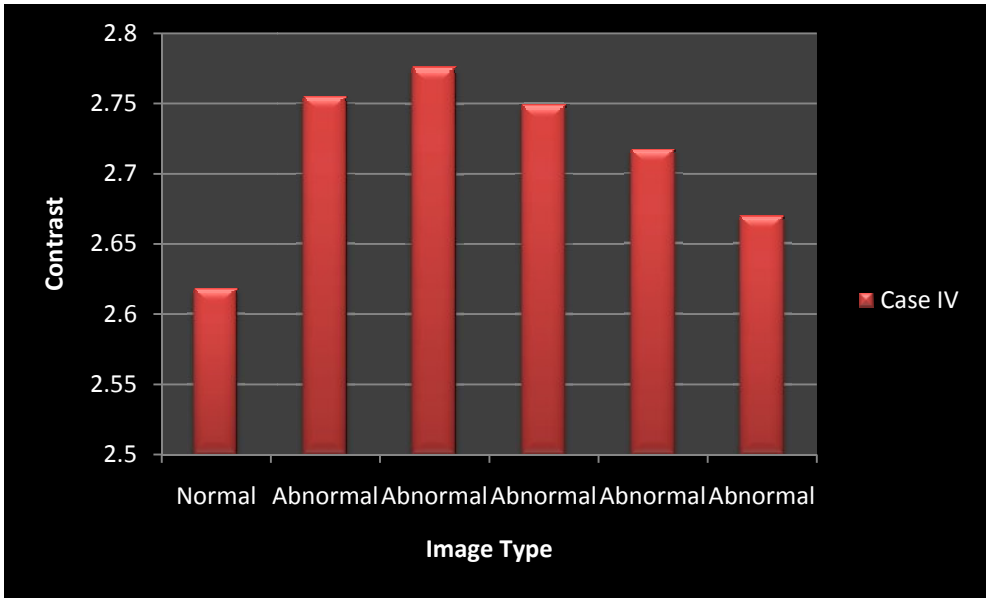

Figure 6.16 Comparison between the contrast of normal and abnormal image

2. CORRELATION

The correlation of the normal image for Case IV is having the maximum value i.e. 0.0196 and is not within the range of the abnormal images.

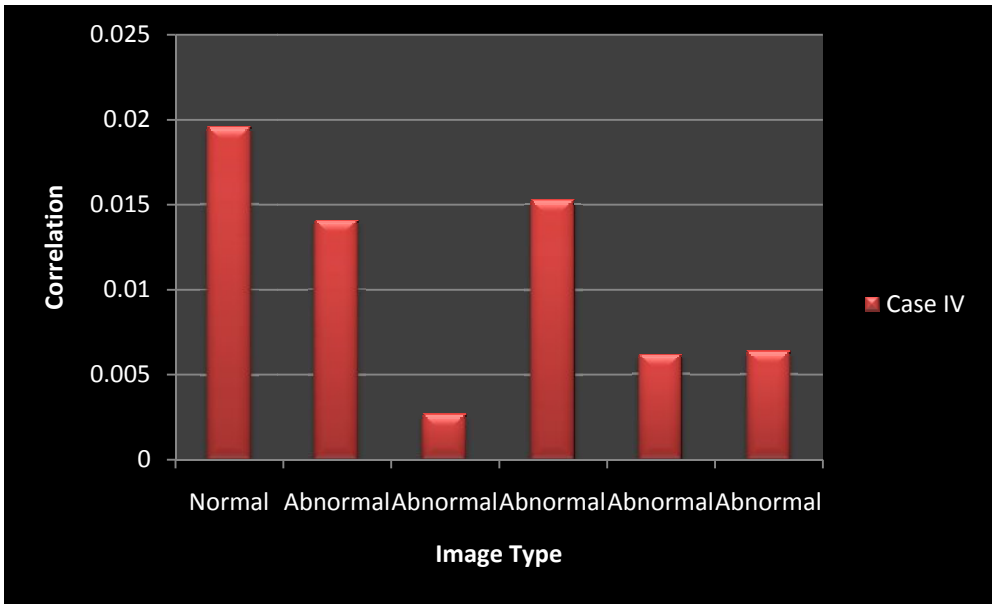

Figure 6.17 Comparison between the correlation of normal and abnormal image

3. ENERGY

The energy of the normal image for Case IV is having the least value i.e. 7.2459 and is not within the range of the abnormal images.

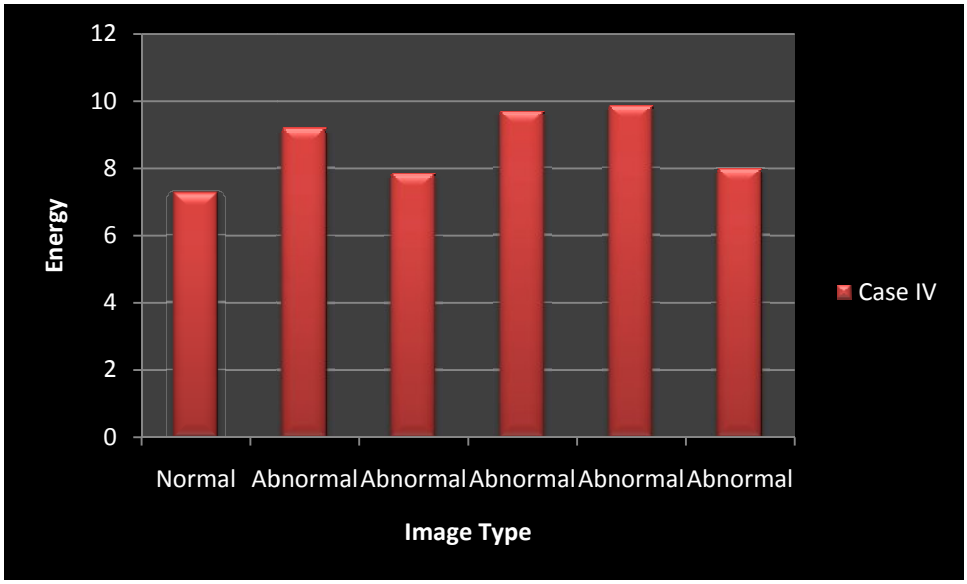

Figure 6.18 Comparison between the energy of normal and abnormal image

4. HOMOGENEITY

The homogeneity of the normal image for Case IV is having the least value i.e. 0.0243 and is not within the range of the abnormal images.

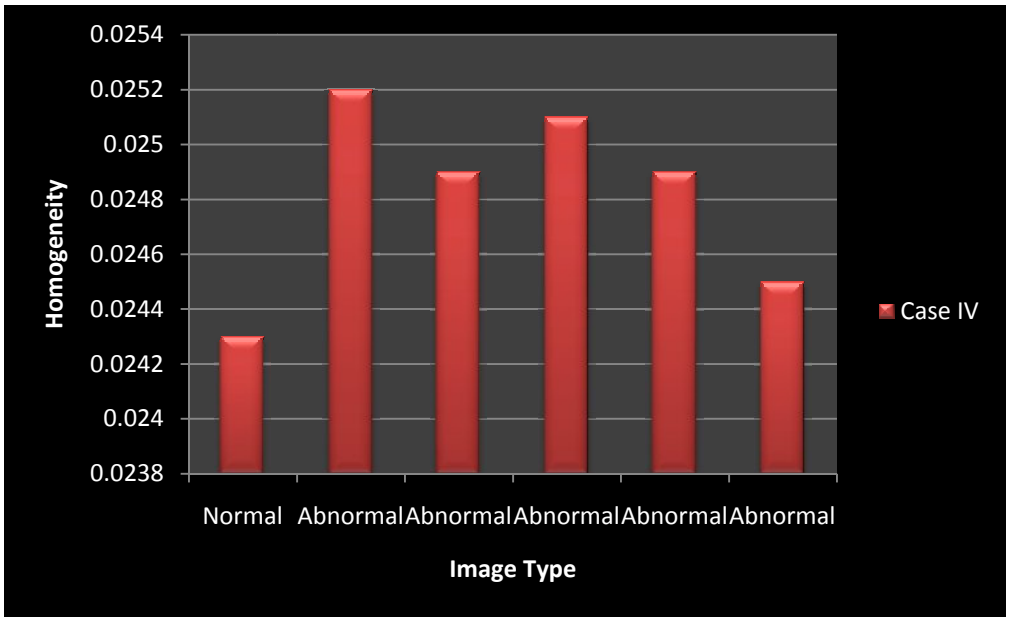

Figure 6.19 Comparison between the homogeneity of normal and abnormal image

5. ENTROPY

The entropy of the normal image for Case IV is having the least value i.e. 7.0265 and is not within the range of the abnormal images.

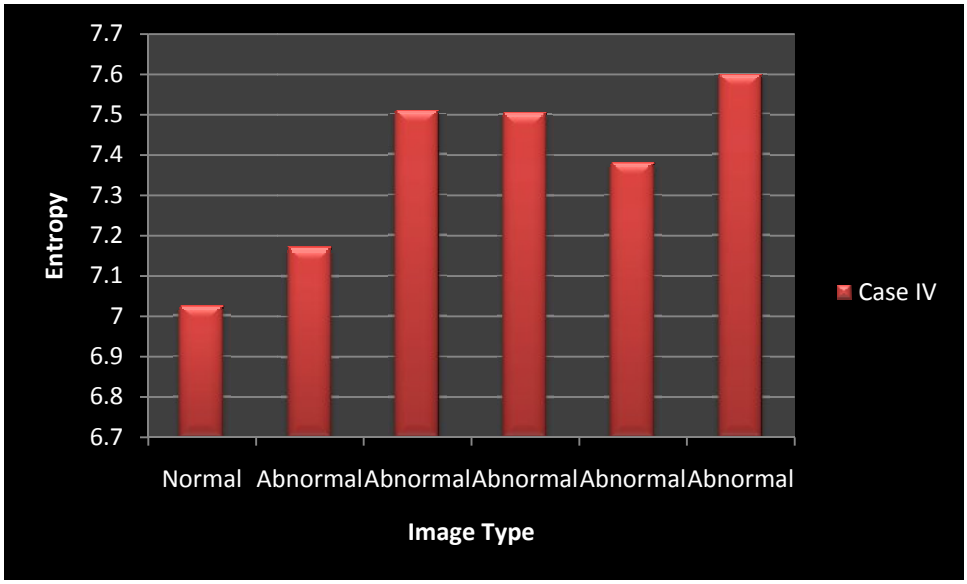

Figure 6.20 Comparison between the entropy of normal and abnormal image

CASE V

1. CONTRAST

The contrast of the normal image for Case V is having the maximum value i.e. 2.6536 and is not within the range of the abnormal images.

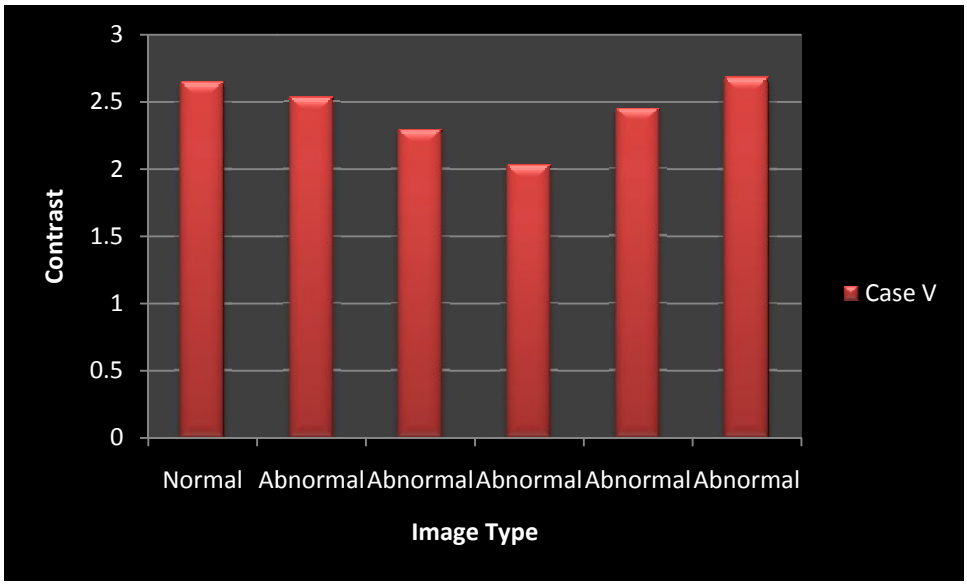

Figure 6.21 Comparison between the contrast of normal and abnormal image

2. CORRELATION

The correlation of the normal image for Case V is having the least value i.e. 0.025 and is not within the range of the abnormal images.

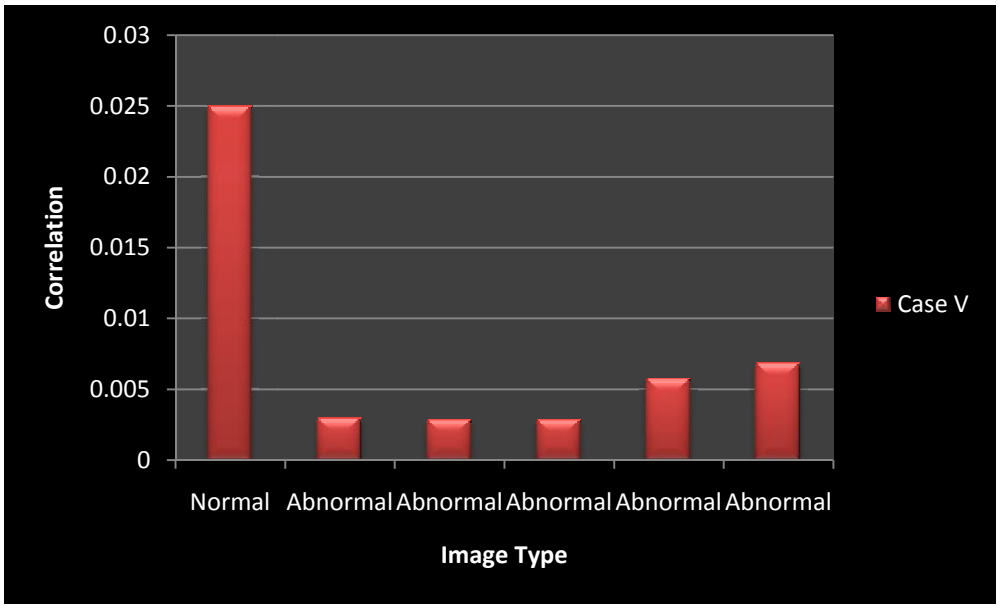

Figure 6.22 Comparison between the correlation of normal and abnormal image

3. ENERGY

The energy of the normal image for Case V is having the least value i.e. 1.127 and is not within the range of the abnormal images.

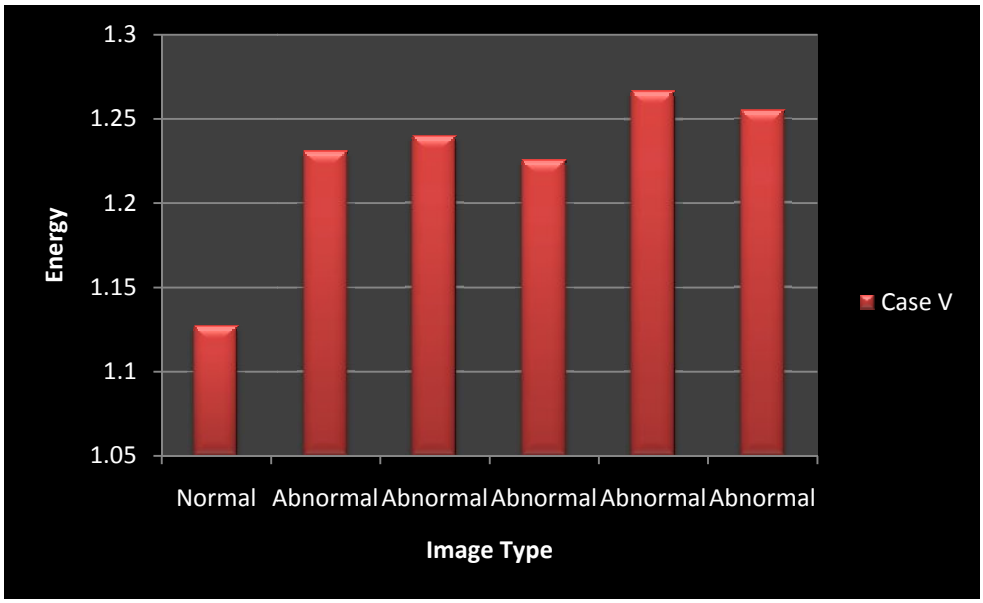

Figure 6.23 Comparison between the energy of normal and abnormal image

4. HOMOGENEITY

The homogeneity of the normal image for Case V is having the least value i.e. 2.0233 and is not within the range of the abnormal images.

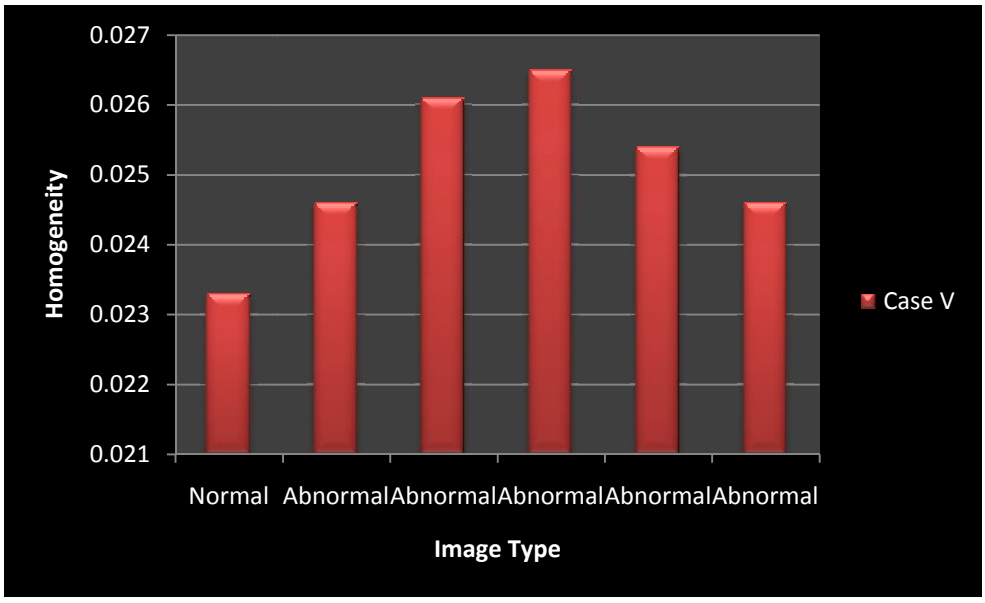

Figure 6.24 Comparison between the homogeneity of normal and abnormal image

5. ENTROPY

The entropy of the normal image for Case V is having the maximum value i.e. 7.4908 and is not within the range of the abnormal images.

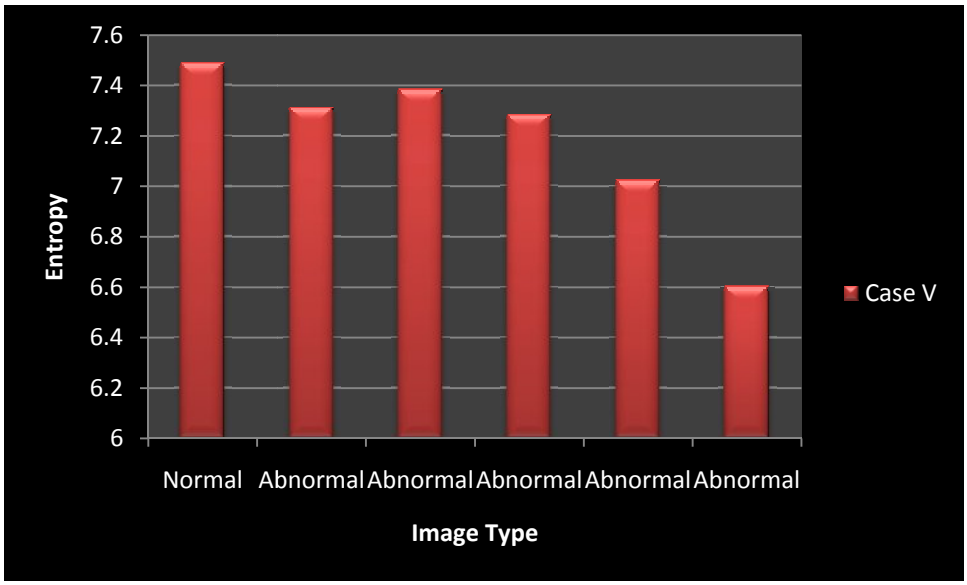

Figure 6.25 Comparison between the entropy of normal and abnormal image

CHAPTER 7
CONCLUSION AND FUTURE SCOPE

CONCLUSION

This thesis provides the analysis of the textures features of MR images. The texture analyses of both the normal and abnormal images are done. On the bases of the values of abnormal images, the range is calculated and further it is compared with the texture features of normal image. So, to determine the whether the abnormality is there or not in the image, its texture features are observed and the feature lying outside the range finally concludes that image is normal.

It is seen that 5 different cases are taken and each case consists of 5 abnormal image and 1 normal image of a particular part of the brain. Texture analysis of the 5 different images of each case is done by finding their contrast, correlation, energy, homogeneity and entropy, and then their range is obtained. Finally, analysis of the normal image of each case is performed. The texture value of particular normal is compared with the range of that particular case. If the value outside the range concludes the normality of the image.

FUTURE SCOPE

In this thesis texture analysis of MR images is performed which subscribed of lesser number of images which may not prove a much accurate result. So, in order to get a better accuracy, large number of images must be taken. The images that here observed are the MR images of the brain of the patients. Different body parts images can also be taken and their analysis can be done. Different scan images can also be taken and their texture analysis can be performed.

REFERENCES

[1] Wu Jianchao , Liao Mengyang, Wang Sixian "Texture segmentation of ultrasound B-scan image by sum and difference histograms" Annual International Conference of the IEEE Engineering in Medicine and Biology Society, Vol. 2, pp. 417-418, 1989.

[2] Kah-Chan Low1 and James M. Coggins "Modified fuzzy c-mean in Medical Image Segmentation" Proceedings on SPIE Symposim on Advances in Biomedical Imaging, Pages 3429-3432, 1999.

[3] N.A.Mohamed, M.N.Ahmed, A.Farag "Modified fuzzy c-mean in medical image segmentation" IEEE International Conference on Medical Imaging, Vol. 6, pp. 3429-3432, 1999.

[4] Koss, J.E. Newman, F.D. Johnson, T.K. Kirch "Abdominal organ segmentation using texture transforms and a Hopfield neural network" Medical Imaging, IEEE Transactions on Medical imaging, Vol. 18, pp. 417-418, 1999.

[5] George York and Yongmin Kim "Ultrasound Processing and Computing: Review and Future Directions" Ultrasound Medical Imaging, Vol. 1, pp. 559-588, 1999.

[6] Ewout Vansteenkiste, Alessandro Ledde, Gjenna Stippel, Bruno Huysmans, Paul Govaert, Wilfried Philips "Segmenting Leukomalacia using Textural Information and Mathematical Morphology" IEEE ProRISC, pp. 441-446, 2003.

[7] Stewart A. Levin, Martijn de Hoop "Extracting information from geophysical, medical, and space images" IEEE International Symposium on Biomedical Imaging, Vol. 21, pp. 245-258, 2002.

[8] Alain Pitiot, Arthur W. Toga and Paul M. Thompson "Adaptive Elastic Segmentation of Brain MRI via Shape-Model-Guided Evolutionary Programming" Image visual Computing, Vol. 33, no. 3, pp. 161–178, 2002.

[9] Zumray, Dokur, Tamer, Olmez "Segmentation of ultrasound images by using a hybrid neural network" Seventh International Conference on Image Processing and its Applications, Vol. 23, pp. 1825 – 1836, 2002.

[10] Djamal Boukerroui, Atilla Baskurt, J. Alison, Oliver Basset "Segmentation of ultrasound images: multiresolution 2D and 3D algorithm based on global and local statistics" Ultrasonic image processing and analysis, Vol. 24, pp. 779 – 790, 2003.

[11] Russell Muzzolinil, Yee-Hong Yang and Roger Pierson "A Multiresolution Texture Segmentation Approach with Application to Diagnostic Ultrasound Images" IEEE Medical Imaging Conference, Santa, pp. 567-578, 2003.

[12] Mohamed, M.M. Abdel-galil, T.K. Salama, M.A. El-Saadany, E.F. Kamel, M. Fenster, A. Downey, D.B. Rizkalla "Prostate cancer diagnosis based on Gabor filter texture segmentation of ultrasound image". IEEE CCECE Canadian Conference on Medical Imaging, Vol. 3, pp. 1485- 1488, 2003.

[13] Stuart S. C. Burnett and George Starkschall, Craig W. Stevens and Zhongxing Liao, "A deformable-model approach to semi-automatic segmentation of CT images demonstrated by application to the spinal canal" International Conference of the IEEE on Engineering in Medicine and Biology Society, Vol. 15, pp. 3401-3404, 2006.

[14] Yongjian Yu, Scott T. Acton and Janelle A. Molloy "Segmentation of the prostate from Magnetic Resonance images" Proceedings of International Conference on Image Processing, Vol. 31, pp. 3474-3484, 2004.

[15] Jun Xie, Yifeng Jiang, Hung-Tat Tsui "Segmentation of kidney from ultrasound images based on texture and shape priors" IEEE Transactions on Medical Imaging, Vol. 24, No. 1, pp. 45-57, 2005.

[16] Barbara Podda and Andrea Giachetti "Texture Analysis of CT Images for Vascular Segmentation: A Revised Run Length Approach" Image Analysis and Processing – ICIAP, 2005, Vol. 3617, pp. 907-914, 2005.

[17] Esmeraldo dos Santos Filho, Makoto Yoshizawa, Akira Tanaka, Yoshifumi Saijo and Takahiro Iwamoto "Moment-based texture segmentation of luminal contour in intravascular ultrasound images" Computer Med Imaging Graphics, pp. 91-99, 2005.

[18] Springer Berlin and Heidelberg "Application of Wavelet Transforms and Bayes Classifier to Segmentation of Ultrasound Images" IEEE Transactions on Medical Imaging Vol. 3523/2005, pp. 336-342, 2005.

[19] S. S. Mohamed" Prostate cancer multi-feature analysis using trans-rectal ultrasound images" IEEE 11th International Conference on Image Processing, pp. 34-56, 2005.

[20] Bassel Abou Merhy, Pierre Payeur, Emil M. Petriu "Unsupervised Texture Segmentation for 2D Probabilistic Occupancy Maps" IEEE International Workshop, pp. 7803-9379, 2005.

[21] Mohsen Ghazel Anthony Traboulsee Rabab K. Ward "Semi-Automated Segmentation of Multiple Sclerosis Lesions in Brain MRI using Texture Analysis" IEEE International Symposium on Signal Processing and Information Technology pp. 6-10, 2006.

[22] Constantino Carlos Reyes Aldasoro and Abhir Bhalerao "Volumetric Texture Segmentation by Discriminant Feature Selection and Multiresolution Classification" IEEE Transactions on Medical Imaging, Vol. 26, No. 1, pp. 187–260, 2007.

[23] Jesus Cerquides, Maite Lopez Sanche, David Masip, Anna Puig, "Classification of biomedical high-resolution micro-CT images for direct volume rendering" Proceedings of the 25th IASTED International Multi-Conference: artificial intelligence and applications, Vol. 23, no.1, pp. 341 - 346 , 2007.

[24] Rushin Shojaii, Javad Alirezaie, Gul Khan, Paul Babyn "Automatic Honeycomb Lung Segmentation in Pediatric MR Images" 9th International Symposium on Image Processing and Its Applications, pp 1-4, 2007.

[25] Cobzas, Dana Birkbeck, Neil Schmidt, Mark Jagersand, Martin Murtha, Albert "3D Variational Brain Tumor Segmentation using a High Dimensional Feature Set" IEEE 11th International Conference on Computer Vision, pp. 1-8, 2007.

[26] Jiahui Wang, Roger Engelmann, and Qiang Li "Segmentation of pulmonary nodules in three-dimensional CT images by use of a spiral-scanning technique" Medical Image Analysis, Vol. 34, pp. 4678-4689, 2007.

[27] Claude, Cariou, Kacem, Chehdi "Unsupervised texture segmentation/classification using 2-D autoregressive modeling and the stochastic expectation-maximization algorithm" IEEE Transaction on Medical Imaging, Vol. 5,pp. 905-917, 2008.

[28] Li Ma, Yajing Shan "Integration of Fractal and Grey-level Features for Texture Segmentation" IEEE Transaction on Image Processing, Vol. 5, pp. 3245-3672, 2008.